Artificial Intelligence-Enhanced Analysis of Echocardiography-Based Radiomic Features for Myocardial Hypertrophy Detection and Etiology Differentiation

Moon, Inki

Department of Medicine
Graduate School
Yonsei University

Artificial Intelligence-Enhanced Analysis of Echocardiography-Based Radiomic Features for Myocardial Hypertrophy Detection and Etiology Differentiation

Advisor Chang, Hyuk-Jae

A Dissertation Submitted
to the Department of Medicine
and the Committee on Graduate School
of Yonsei University in Partial Fulfillment of the
Requirements for the Degree of
Doctor of Philosophy in Medical Science

Moon, Inki

June 2025

Artificial Intelligence-Enhanced Analysis of Echocardiography-Based Radiomic Features for Myocardial Hypertrophy Detection and Etiology Differentiation

This Certifies that the Dissertation Of Moon, Inki is Approved

Committee Chair	**Jung, In Hyun**
Committee Member	**Chang, Hyuk-Jae**
Committee Member	**Yoon, Yeonyee**
Committee Member	**Chun, Eun Ju**
Committee Member	**Sung, Ji Min**

Department of Medicine
Graduate School
Yonsei University
June 2025

TABLE OF CONTENTS

LIST OF FIGURES

LIST OF TABLES

ABSTRACT

Artificial Intelligence-Enhanced Analysis of Echocardiography-Based Radiomic Features for Myocardial Hypertrophy Detection and Etiology Differentiation

While echocardiography is pivotal for detecting left ventricular hypertrophy (LVH), it struggles with etiology differentiation. To enhance LVH assessment, we aimed to develop an artificial intelligence (AI) algorithm using echocardiography-based radiomics. This algorithm is designed to detect LVH and differentiate its common etiologies, such as hypertrophic cardiomyopathy (HCM), cardiac amyloidosis (CA), and hypertensive heart disease (HHD), based on echocardiographic images.

The developmental datasets were sourced from diverse medical centers (867 subjects), while an independent external validation set was obtained from a single tertiary medical center (619 subjects). Utilizing radiomic feature analysis on four fundamental echocardiographic views, conventional and harmonization-driven myocardial textures were extracted. Myocardial geographic features, such as myocardial shape and thickness, were also utilized as key variables. The classification algorithm was developed, and the contribution of each variable was evaluated by Shapley Additive Explanations.

In internal validation, the classification model reliably detected LVH with an area under the curve (AUC) of 1.00 (95% confidence interval [CI], 1.00–1.00). The model demonstrated strong performance in differentiating etiologies, achieving AUCs of 0.97 (95% CI, 0.94–0.99) for HCM, 0.95 (95% CI, 0.90–0.99) for CA, and 0.86 (95% CI, 0.78–0.93) for HHD. In external validation, these results were consistent, with AUCs of 0.96 (95% CI, 0.92–0.98) for HCM, 0.89 (95% CI, 0.83–0.93) for CA, and 0.86 (95% CI, 0.81–0.91) for HHD. Notably, harmonization-driven textures played a key role in differentiating HCM, while conventional textures and myocardial thickness were influential in differentiating CA and HHD.

This study confirms that AI-enhanced echocardiography-based radiomics effectively identifies LVH and its etiologies, highlighting the potential of AI-driven texture and geographic analysis in LVH evaluation.

Key words : Echocardiography-based radiomics, artificial intelligence, left ventricular hypertrophy

1. INTRODUCTION

Left ventricular hypertrophy (LVH) is commonly observed in clinical settings, often signaling a range of cardiovascular diseases and thus substantially impacting morbidity and mortality.[1-3] LVH is typically identified through imaging studies, with echocardiography being the most commonly employed non-invasive modality. While echocardiography provides essential data on left ventricular (LV) mass, wall thickness, and cardiac function, it alone may not precisely pinpoint the etiological factor of LVH, which is crucial for specific treatment plans and outcome prediction.[4,5] Because the morphological and functional characteristics of LVH observed on echocardiography are substantially influenced by specific diseases and depend on the stage of disease, it could become a similar pattern. Additionally, the subjective nature and variability in echocardiographic interpretation necessitate advanced techniques like magnetic resonance imaging or endomyocardial biopsy for deeper etiological insights.[6]

Artificial intelligence (AI) technology has rapidly evolved, introducing a range of sophisticated methods for analyzing images. Echocardiography, which provides dynamic, high-resolution images of the heart, represents a valuable data source ripe for advanced computational analysis. In response to previous challenges, there has been a significant shift towards utilizing AI to assist in the echocardiographic analysis and categorization of LVH etiology. [7,8] Deep learning (DL), a subset of AI, has been at the forefront of this revolution. It employs neural networks, particularly convolutional neural networks (CNNs), to automatically learn and identify patterns within large datasets without the need for explicit feature extraction by human operators. In the context of echocardiography, DL models have demonstrated the potential to automate tasks such as segmentation, measurement of cardiac structures, and even the differentiation of various LVH etiologies. However, DL-based methods, while seemingly accurate in differentiating LVH etiologies, often fail to disclose which specific echocardiographic features are used for this differentiation, leaving a significant gap in our understanding and application of AI.[9-11] Additionally, many of these studies lacked external validation or showed significantly reduced performance when evaluated using external datasets.

To overcome the interpretability and validation challenges associated with DL, radiomics has emerged as a complementary approach. Radiomics involves the extraction of a large number of

quantitative features from medical images, which capture a wide array of characteristics such as texture, shape, and intensity.[12] These features can reveal subtle patterns that are not easily discernible by the human eye but may correlate strongly with underlying pathological processes. In echocardiography, radiomics provides a powerful tool for dissecting the complex myocardial textures and patterns associated with various LVH etiologies. By quantifying these features, radiomics allows for a more granular analysis that can enhance diagnostic precision beyond what conventional imaging and even deep learning alone can achieve.

Addressing these challenges, the current study leveraged echocardiography-based radiomics to develop a sophisticated algorithm that not only diagnoses LVH but also differentiates its various etiologies, such as hypertrophic cardiomyopathy (HCM), cardiac amyloidosis (CA), and hypertensive heart disease (HHD). We also examined which features play crucial roles in diagnosing each condition through Shapley Additive Explanations (SHAP) analysis. Importantly, we employ a novel harmonization technique for vendor-independent analysis of myocardial texture features from echocardiographic images, enabling more accurate assessments and enhancing the clinical applicability of our algorithm.

2. METHODS

2.1. Study Dataset

This study utilized extensive echocardiography datasets from multiple Korean medical centers, collected through a collaboration among four sources: (1) the Open AI Dataset Project (AI-Hub) by the Ministry of Science and ICT, South Korea,[13] (2) Korea National Standard Cardiovascular Database and Reference,[14] (3) Seoul National University and Bundang Hospital LVH registry,[9] and (4) Echocardiographic Characteristics for Diagnosis of Infiltrative Cardiomyopathy (ACREDIT) registry (NCT 05108168). From this consolidated dataset, echocardiographic data for patients with normal, HCM, CA, and HHD conditions were extracted. The detailed clinical inclusion criteria for each clinical condition are provided in Table 1.

To facilitate the development and validation of our algorithm, we organized the datasets according to hospital origin. We constructed the developmental dataset from a variety of hospitals, specifically excluding Seoul National University Bundang Hospital (SNUBH). We evaluated 2,285 subjects from Severance Hospital, Seoul National University Hospital, Soonchunhyang University Bucheon Hospital, and other hospitals for eligibility, with 1,171 subjects fulfilling the clinical inclusion criteria (Fig. 1). To evaluate our algorithm's generalization capability, we prepared an independent external validation set from SNUBH, where 1,410 patients were evaluated for eligibility, and 713 met the clinical inclusion criteria (Fig. 1).

This study complied with the ethical guidelines of the Declaration of Helsinki and was approved by each institution's Institutional Review Board (IRB). Due to the study's retrospective design and the minimal impact on subjects, the IRB waived the need for informed consent. Additionally, the research was carried out following the Proposed Requirements for Machine Learning Evaluation in Cardiovascular Imaging.[15]

Table 1. Clinical Inclusion and Exclusion Criteria

Conditions	Definition*
Normal	(1) no clinical history of cardiovascular disease or diabetes; (2) normal blood pressure (≤130/80 mmHg); (3) body mass index ≤30 kg/m2; (4) normal sinus rhythm at 50–85 beats/min without conduction abnormalities; (5) normal LV wall thickness and LV wall motion; (6) normal left atrial size (left atrial volume index <27 mL/m2 using the biplane method of discs) or left atrial dimension <40 mm; (7) no mitral valve prolapse; and (8) no more than trivial valve regurgitation
HCM	(1) end-diastolic LVWT max ≥15 mm on echocardiography, (2) definite evidence of HCM on cardiac magnetic resonance (CMR) or a typical gene mutation on genetic analysis, and (3) absence of abnormal loading conditions that could sufficiently explain the LVH
CA	(1) definite evidence of amyloid involvement either through on endomyocardial biopsy (Congo-Red positive and amyloid P positive on immunohistochemistry) or by demonstrating amyloidosis on extra-cardiac biopsy with cardiac involvement supported by CMR or pyrophosphate scans, and (2) end-diastolic LVWTmax ≥12 mm
HHD	(1) history of hypertension; (2) left ventricular (LV) mass index [LVMI] >115 g/m2 in men, LVMI >95 g/m2 in women; (3) end-diastolic maximal LV wall thickness (LVWTmax) ≥12 mm; (4) Regression of LVH after appropriate blood pressure control; and (5) exclusion of other causes of LVH (such as HCM, infiltrative cardiomyopathy, metabolic cardiomyopathy, etc.)

*Patients must meet all the following criteria

Abbreviations: CA, cardiac amyloidosis; HCM, hypertrophic cardiomyopathy; HHD, hypertensive heart disease

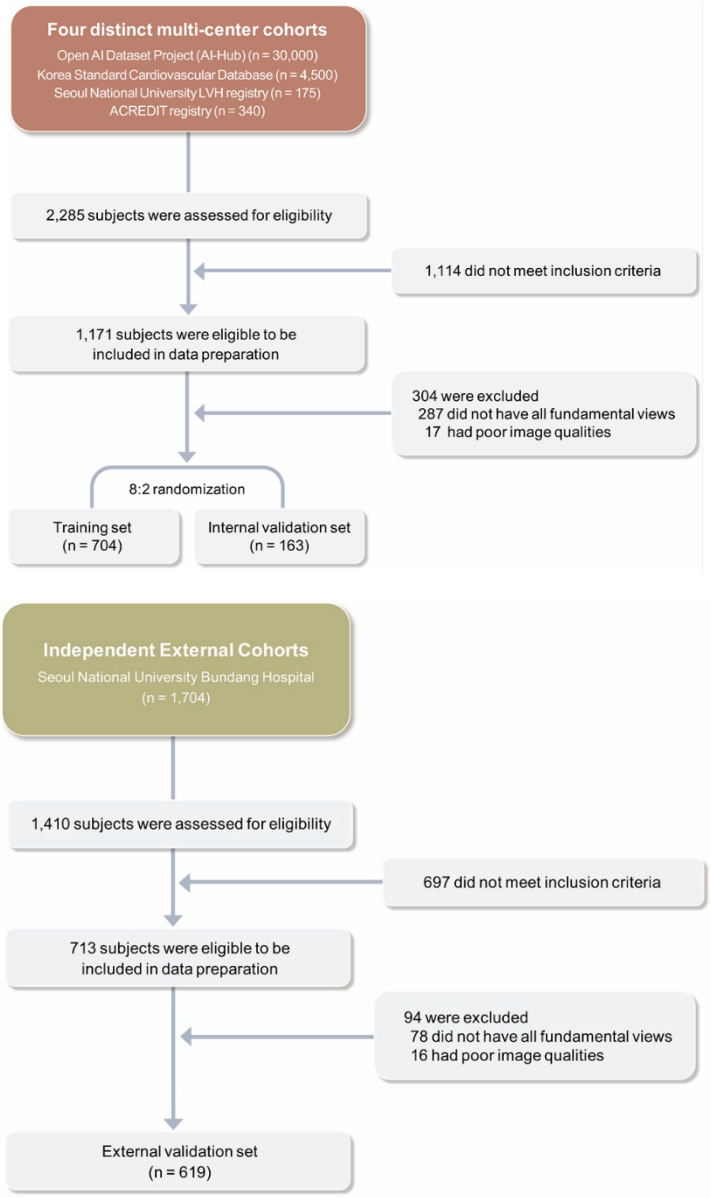

Fig. 1. Flow Chart of Data Preparation Process: Developmental and External Validation Dataset

Abbreviations: ACREDIT, Echocardiographic Characteristics for Diagnosis of Infiltrative Cardiomyopathy registry; AI, artificial intelligence; LVH, left ventricular hypertrophy.

2.2. Data Preparation

In this study, our algorithm was designed to extract and analyze myocardial features from images of the end-diastolic (ED) and end-systolic (ES) phases within the four fundamental views of echocardiography: parasternal long-axis (PLAX), parasternal short-axis at mid-level (PSAX), apical 4-chamber (A4Ch), and apical 2-chamber (A2Ch). To achieve this, we initially employed our previously developed AI-based echocardiographic automatic analysis system (Sonix Health, Ontact Health, Korea) to select the necessary views and identify the ED and ES images within those views.[16] The deep learning (DL)-based segmentation algorithm has been detailed in our previous research, highlighting its robust performance in the LV cavity, myocardium, and left atrial cavity segmentation.[17,18] This system utilizes a 3-dimensional (2D + time) convolutional neural network (CNN) trained through semi-supervised learning, combining supervised learning based on expert-annotated ground truth with unsupervised learning for motion estimation via a spatial transformer network.[19] This combined approach enabled the model to capture and interpret essential cardiac motion patterns accurately. The proposed algorithm is highly robust to image quality, through echo-specific data augmentation,[20] such as haze and shadow artifacts, as well as a variety of general data augmentation techniques.

The segmentation model was specifically trained and optimized for multiple echocardiographic views, including the apical 4-, 2-, and 3-chamber views (A4C, A2C, and A3C), parasternal long-axis view (PLAX), and the parasternal short-axis view (PSAX). Each echocardiographic view required a distinct model component to accommodate the unique anatomical and imaging characteristics of the view, even though the overall network architecture remained consistent across views. By processing these various views, our DL-based segmentation algorithm delivers highly accurate segmentation results, ensuring clinical reliability and robust performance across diverse imaging conditions. As a result, it can provide detailed and clinically relevant segmentation of cardiac structures, which is critical for extracting radiomic features. The system's comprehensive architecture is shown in Fig. 2. Representative cases of successful segmentation included in this study and failed segmentations excluded from the study are provided in Fig. 3 and 4.

After the initial processing, cases missing any of the four fundamental views, poor image quality leading to inaccurate ED/ES phase detection, and those with failed segmentation were excluded

(Fig. 1). The study's developmental dataset included 867 cases across various conditions: 276 with HCM, 168 with CA, 135 with HHD, and 288 normal subjects. The data were split 8:2 for training and testing to ensure homogeneity, with 704 for training and 163 for internal validation. Similarly, the external validation set included 619 patients: 46 with HCM, 66 with CA, 93 with HHD, and 414 normal subjects. The process was validated by experienced cardiologists.

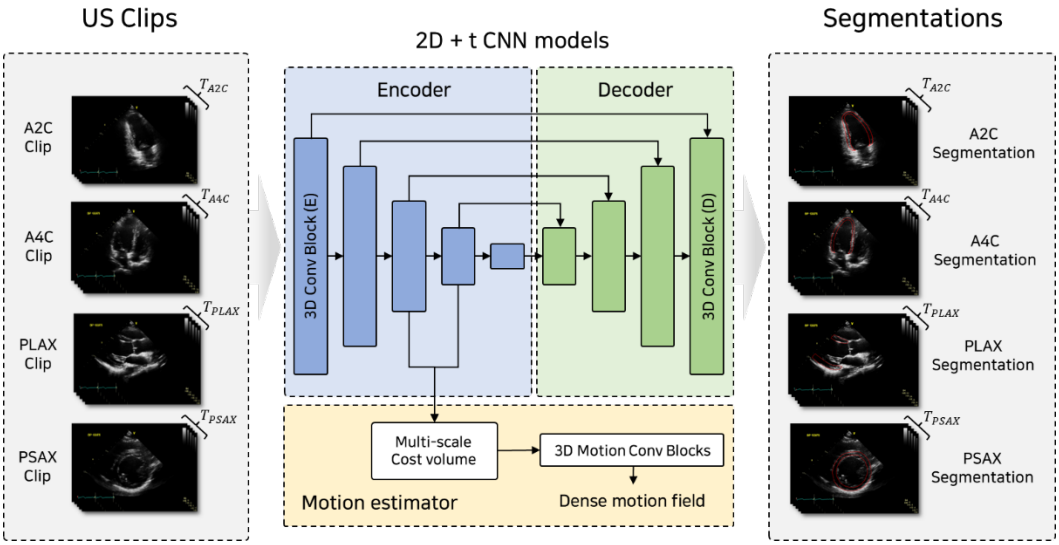

Fig. 2. Architecture of AI-based Left Ventricular Myocardium Segmentation System. The figure depicts the architecture of the AI-based segmentation system, illustrating the flow from the input of various echocardiographic views (including the apical views, PLAX, and PSAX) to the segmentation output for each view. This design allows the system to produce precise delineations of the left ventricular myocardium across different echocardiographic views, accommodating each view's unique features and imaging characteristics.

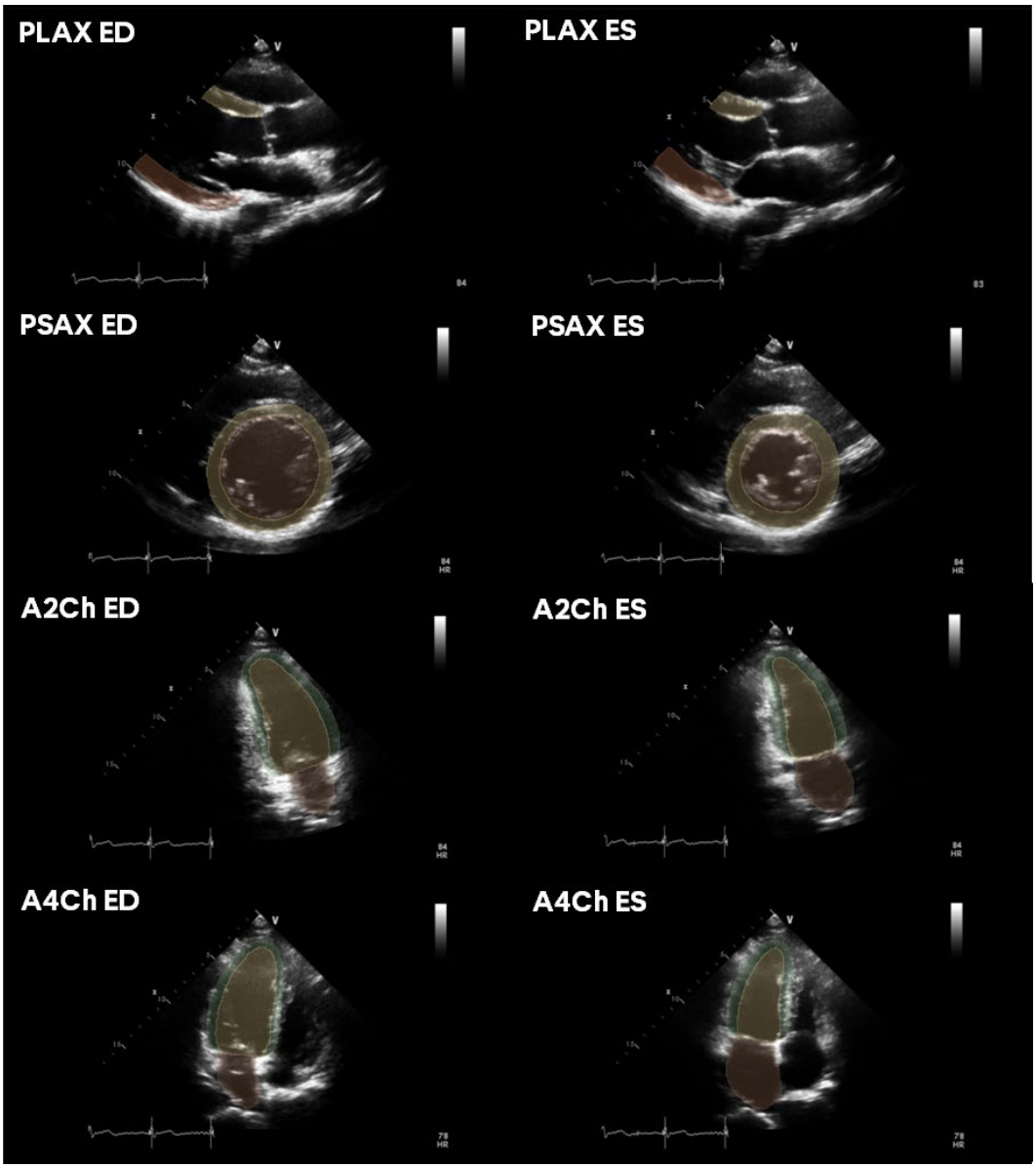

Fig. 3. Representative Case of Segmentation. The images capture the ED and ES phases, demonstrating the system's precision in delineating the LV myocardium across cardiac phases.

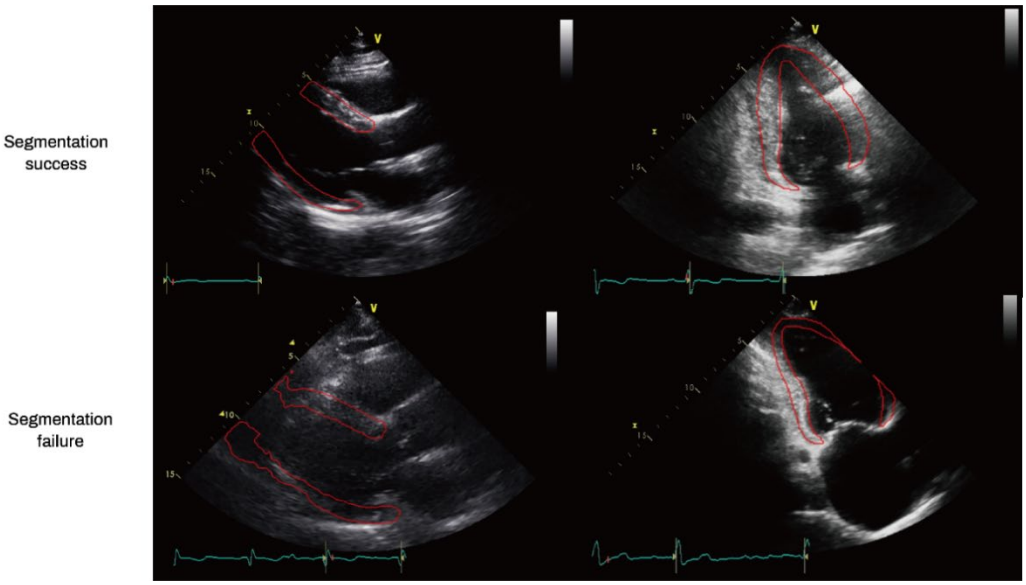

Fig. 4. Representative Cases of Inclusion and Exclusion Cases. In our study, we utilized the AI-based system we developed to perform automatic segmentation and extract radiomics features from the segmented LV myocardium. The upper cases represent successful segmentation instances, whereas the lower cases show instances where segmentation failed and were thus excluded. From the upper cases, it can be observed that segmentation was successful even with relatively poor image quality. Conversely, the lower cases illustrate that segmentation failed in situations where the image quality was inferior, making it difficult even for human experts to perform segmentation or where the LV myocardium extended beyond the image boundaries.

2.3. Myocardial Feature Extraction

We delved into quantitative features by extracting texture and geographic features from each segmented LV myocardium, employing the well-established open-source Python package Pyradiomics.[21] For a clearer understanding and effective management of the diverse features, we organized them into the four following categories (Fig. 5).

2.3.1. Conventional Texture Features (F1) and Harmonization-driven Texture Fearutres (F2)

For conventional texture features (F1), we extracted the 91 core features consist of 18 first-order statistical features, 22 co-occurrence matrices, 16 gray-level run length matrices, 16 gray-level size zone matrices, 14 gray-level dependence matrices, and 5 texture features based on neighboring gray-level difference matrices. And we extracted additional set of 91 features from 16 conventional filtered images. Consequently, we defined a set of 1,547 features as the conventional texture feature set. Next, we additionally applied a novel harmonization technique developed by our team to derive harmonization-driven texture features (F2). We filtered the echocardiography image with 2D convolution kernels in the first layer of fine-tuning ConvNext-V2 network,[22] and extracted 91 core feature sets from the filtered image.This technique was designed to reduce vendor-specific speckle pattern variability in LV myocardium.[23]

2.3.2. Geographic Features (Myocardial Shape [F3] and Thickness [F4])

We also included geographic features, myocardial shape (F3) and thickness (F4). We extracted 13 shape features, which were supported by Pyradiomics Package, at four fundamental views, producing 52 shape features. Furthermore, considering that LVH is typically diagnosed by measuring the thickness of the left ventricular wall, we included myocardial thickness as an input for the machine-learning model. We measured six myocardial thicknesses in the following segments: apical lateral wall, apical septum, mid-inferior septum, mid-anterior lateral wall, basal anterior-lateral wall, and basal inferior septum, and the myocardial thickness at both the ED and ES phases. We used the average

thickness values for each segment if measurements were available from both A2Ch and A4Ch. In addition, we measured three 2-dimensional diameters in the PLAX view: LV septum, LV cavity, and LV posterior wall. Thus, we extracted 61 myocardial geographic features for each cardiac phase.

2.3.3. Percent Change ([%Δ]) Between Phases and Total Packages of Myocardial Features

We initially extracted 1,638 texture features (1,547 conventional and 91 harmonization-driven features) from each view. The features were extracted from four fundamental views, resulting in 6,552 features (1,547 features × 4 views). This feature set was extracted in both end-diastolic (ED) and end-systolic (ES) phases, resulting in 13,104 features (6,552 features × 2 phases). And, the total number of geographic features from each phase was 122 (61 features × 2 phases).

To maximize the performance, we computed the variation in the extracted features. All features were derived from both the ED and ES phases, and the percentage change for each feature was calculated using the formula (ES-ED)/ED. This percent change calculation approach is based on the premise that heart muscle movements vary across different diseases, and such a calculation could numerically represent these variations. This method enabled us to utilize features to capture specific changes that occur throughout the cardiac cycle. Therefore, we calculated the percentage changes for the 6,552 texture features and 61 geographic features between the ED and ES phases.

Consequently, the final conventional and harmonization-driven texture feature set consisted of 19,656 features (13,104 texture features and 6,552 percent changes). Likewise, for texture feature extraction, there were 183 geographic features (122 geographic features and 61 percent changes). In total, we utilized 19,839 features for LVH detection and etiology differentiation modeling.

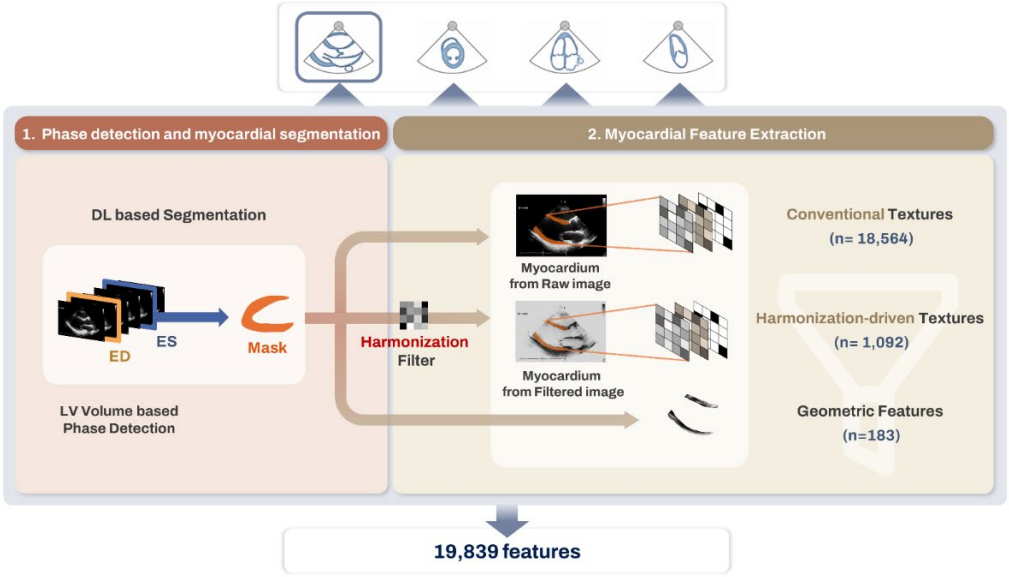

Fig. 5. Automated Process of Echocardiographic Feature-Extraction for Developing the Classification Model. The automated software first detected end-diastolic and end-systolic phases and then segmented LV myocardium from four distinct echocardiographic views. In extracting texture features, both conventional text features and newly developed harmonization-driven texture features were obtained using advanced filters. Geographic features encapsulating myocardial shape and thickness were also extracted. Upon combining data across all views and phases, a total of 19,839 features were extracted and utilized to develop the classification model. Abbreviations: DL, deep-learning; ED, end-diastole; ES, end-systole; LV, left ventricular.

2.4. Feature Selection and Classification Modeling

2.4.1. Feature Selection

We selected features with a strong impact on classification targets, encompassing the features of conventional and harmonization-driven textures, shapes, thickness features, and feature change rates. Four binary classification models were built: 1) LVH versus normal, 2) HCM versus (CA and HHD), 3) CA versus (HCM and HHD), and 4) HHD versus (HCM and CA). By utilizing these four classification models hierarchically, we can distinguish between four classes: normal, HCM, CA, and HHD (Fig. 6A). Once classified as LVH, the patient could be further classified as HCM, CA, or HHD, and if all three classification models classified the patient as negative, the patient was designated as "Others."

Features selection was performed using the Boruta and XGBoost algorithms.[24] The Boruta algorithm was used to select the top-ranked features associated with targets.[25] The importance ranking for each variable was calculated with the Boruta algorithm, and the top-ranked features, rank 1, were selected as candidates for modeling. The XGBoost algorithm, which combines multiple weak classifiers to assemble a single robust classifier, was used to select the essential features and machine-learning modeling.[26] XGBoost ranks features by "gain" which represents the fractional contribution of each feature to the model based on the total gain of the splits of that feature. We excluded features with no information gain.

After feature selection, we trained the classification models using the LightGBM algorithm,[27] a widely used gradient-boosting decision-tree learning algorithm. To optimize the performance of our model, we conducted a grid search for hyperparameters. The optimal parameters that yielded the best results for the internal validation dataset were used. The grid search included tuning key parameters, such as n_estimators, learning_rate, max_depth, num_leaves, and boosting_type, to find the optimal combination. To overcome the class imbalance problem, we employed the synthetic minority oversampling technique.[28]

Table 2 summarizes the number of features selected in the four trained models and specific features used in each classification model are as below (Table 3).

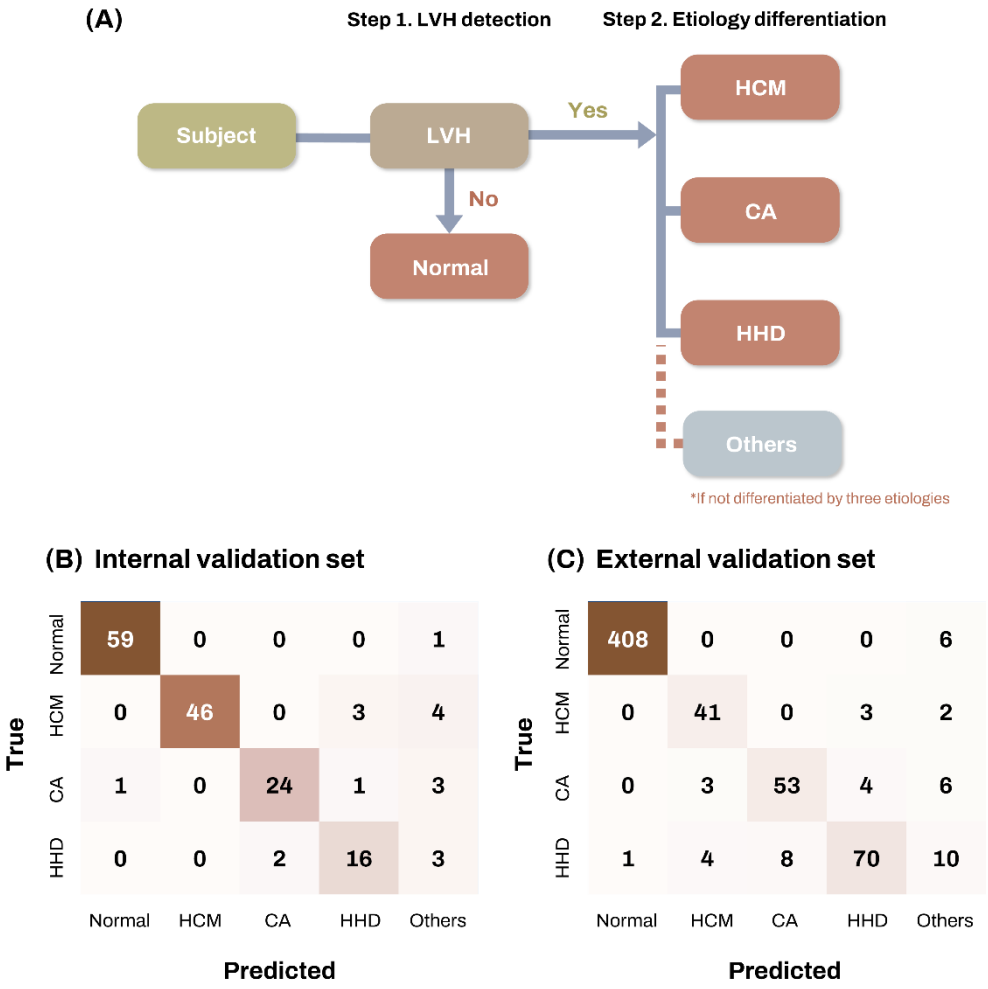

Abbreviations: CA, cardiac amyloidosis; HCM, hypertrophic cardiomyopathy; HHD, hypertensive heart disease; LVH, left ventricular hypertrophy.

Table 2. Selected Features in the Four Classification Models

	Total	F1	%ΔF1	F2	%ΔF2	F3	%ΔF3	F4	%ΔF4
LVH	70	14	9	24	6	6	4	7	0
HCM	82	28	28	13	5	0	0	7	1
CA	83	46	13	7	9	1	2	4	1
HHD	6	2	0	0	0	2	0	2	0

Abbreviation: CA, cardiac amyloidosis; F1, conventional texture; F2, harmonization-driven texture; F3, myocardial shape; F4, myocardial thickness; %Δ, percent change between end-diastole and end-systole; HCM, hypertrophic cardiomyopathy; HHD, hypertensive heart disease; LVH, left ventricular hypertrophy

Table 3.1 Echocardiography-Based Radiomic Features used in LVH differentiation

	Radiomic Features
Conventional texture feature (F1), and %ΔF1	A2CH_ED_wavelet-HHL_ngtdm_Strength, wavelet-LHL_gldm_ SmallDependenceLowGrayLevelEmphasis A4CH_ED_wavelet-HLL_glrlm_RunLengthNonUniformityNormalized A4CH_ES_wavelet-LHL_firstorder_Mean, wavelet-LLL_glszm_ LargeAreaLowGrayLevelEmphasis A4CH_rate_wavelet-HLL_glrlm_GrayLevelNonUniformity, wavelet-LHH_ gldm_DependenceNonUniformity, GrayLevelNon Uniformity, glszm_SmallAreaEmphasis PSAX_ED_glcm_Imc2, wavelet-HLL_glrlm_ RunLengthNonUniformityNormalized PSAX_ES_wavelet-HLH_gldm_LargeDependenceEmphasis Gabor_A2CH_ES_firstorder_Skewness, rate_glszm_SizeZoneNon Uniformity, PLAX_ED_glrlm_LowGrayLevelRunEmphasis LoG_PLAX_ES_glcm_Imc2, PSAX_rate_firstorder_Mean, A4CH_ED_ firstorder_Skewness, firstorder_Median, ES_firstorder_Kurtosis, PSAX_rate_firstorder_Mean, Uniformity, glrlm_LongRun Emphasis
Harmonization-driven texture features (F2), and %ΔF2	A2CH_ED_firstorder_TotalEnergy, glrlm_RunLengthNon Uniformity, glszm_SmallAreaEmphasis, ES_glrlm_RunEntropy, RunLengthNonUniformityNormalized, rate_glrlm_GrayLevelNonUniformity, ngtdm_Strength A4CH_ED_firstorder_TotalEnergy, Entropy, glcm_Correlation, glrlm_RunLengthNonUniformity, RunLengthNonUniformity, ES_glrlm_RunLengthNonUniformity, glszm_ZoneEntropy, rate_gldm_LargeDependenceEmphasis, glszm_ZonePercentage PLAX_ES_firstorder_TotalEnergy, glszm_GrayLevelNonUniformity, LowGrayLevelZoneEmphasis, ngtdm_Coarseness, rate_glrlm_GrayLevelNonUniformity, ED_firstorder_TotalEnergy, glrlm_RunEntropy, RunLengthNonUniformity

	PSAX_ES_firstorder_TotalEnergy, Entropy, glrlm_RunEntropy, RunLengthNonUniformity, RunLengthNonUniformityNormalized, rate_gldm_GrayLevelNonUniformity
Myocardial shape (F3), and %ΔF3	A2CH_rate_Maximum3Ddiameter A4CH_ED_Maximum2DdiameterColumn, Maximum2DdiameterRow, Sphericity, rate_Maximum3Ddiameter PLAX_ED_SurfaceVolumeRatio PLAX_ES_MeshVolume, SurfaceVolumeRatio, rate_Sphericity, Maximum2DDiameterSlice
Myocardial thickness (F4), and %ΔF4	ED_baseL, baseR, midL, ES_apexR, ES_baseL, PLAX_ IVSd, LVPWd

Abbreviation: A2CH, apical 2-chamber; A4CH, apical 4-chamber; ED, end-diastole; ES, end-systole; IVSd, diastolic interventricular septum; LVH, left ventricular hypertrophy; LVPWd, diastolic left ventricular posterior wall; PLAX, parasternal long-axis, PSAX, parasternal short-axis at mid-level

Table 3.2 Echocardiography-Based Radiomic Features used in HCM differentiation

	Radiomic Features
Conventional texture feature (F1), and %ΔF1	A2CH_ED_glszm_LargeAreaHighGrayLevelEmphasis, ES_wavelet-LLH_ngtdm_Busyness, rate_glrlm_GrayLevelNonUniformity, glszm_LargeAreaHighGrayLevelEmphasis A4CH_ED_wavelet-HHH_gldm_GrayLevelNonUniformity, wavelet-LLH_gldm_LargeDependenceHighGrayLevelEmphasis, ES_wavelet-HLH_glszm_SizeZoneNonUniformity, SizeZoneNonUniformity Normalized, wavelet-HLL_gldm_LargeDependenceEmphasis, rate_wavelet-HLH_glszm_LowGrayLevelZoneEmphasis, wavelet-LHL_glrlm_ GrayLevelVariance, wavelet-LLL_firstorder_Maximum PLAX_ED_wavelet-HLL_glrlm_RunLengthNonUniformityNormalized, wavelet-LHH_firstorder_Skewness, wavelet-LHL_firstorder_Kurtosis, ES_wavelet-HLL_glrlm_RunLengthNonUniformityNormalized,

	rate_glcm_DifferenceVariance, Id, glrlm_GrayLevelNonUniformity Normalized, wavelet-HHL_firstorder_Skewness, wavelet-LHL_glcm_ MaximumProbability, wavelet-LLL_glszm_LargeAreaHighGrayLevel Emphasis, SizeZoneNonUniformityNormalized PSAX_ED_wavelet-HHH_glszm_HighGrayLevelZoneEmphasis, LowGrayLevelZoneEmphasis, ES_wavelet-HHH_gldm_Dependence Variance, glrlm_ShortRunEmphasis, ngtdm_Contrast, wavelet-HLH_gldm_DependenceEntropy, rate_wavelet-HLH_gldm_ LargeDependenceEmphasis, wavelet-HLL_gldm_LowGrayLevelEmphasis Gabor_A2CH_ED_firstorder_TotalEnergy, ES_gldm_GrayLevelNonUniformity, A4CH_ES_glcm_ClusterShade, PLAX_rate_ngtdm_Busyness, PSAX_rate_glszm_LargeAreaHighGray LevelEmphasis, A2CH_rate_glrlm_ShortRunLowGrayLevelEmphasis, ngtdm_Contrast, A4CH_rate_firstorder_RobustMeanAbsoluteDeviation, PLAX_ES_glszm_GrayLevelNonUniformityNormalized, PSAX_rate_firstorder_Range, PSAX_rate_glcm_Imc1, A4CH_rate_glcm_ Imc1, glcm_JointEntropy, A4CH_ED_firstorder_Skewness, ES_firstorder_Maximum, glcm_ClusterShade, PLAX_rate_ngtdm_Busyness LoG_PLAX_rate_glrlm_LowGrayLevelRunEmphasis, A4CH_ES_firstorder_Minimum, PLAX_ED_gldm_ SmallDependenceLowGrayLevelEmphasis, A2CH_rate_ngtdm_ Complexity, PSAX_ES_glcm_Correlation, A4CH_ED_firstorder_ RobustMeanAbsoluteDeviation, A4CH_rate_glrlm_ HighGrayLevelRunEmphasis, LowGrayLevelRunEmphasis
Harmonization-driven texture features (F2), and %ΔF2	A2CH_ED_firstorder_TotalEnergy, ES_glszm_SmallAreaEmphasis A4CH_ED_firstorder_TotalEnergy, Entropy, ES_glrlm_RunEntropy, rate_glrlm_GrayLevelNonUniformity, RunLengthNonUniformity Normalized, glszm_LowGrayLevelZoneEmphasis PLAX_ED_glrlm_RunEntropy, ES_glrlm_RunEntropy, rate_glrlm_ShortRunEmphasis

	PSAX_ED_glrlm_RunEntropy, RunLengthNonUniformity, RunLengthNonUniformity, RunEntropy, RunLengthNonUniformity Normalized, ES_glszm_HighGrayLevelZoneEmphasis, rate_glcm_Idn
Myocardial shape (F3), and %ΔF3	-
Myocardial thickness (F4), and %ΔF4	ED_apexL, midL, ES_apexL, apexR, rate_baseL, PLAX_IVSs, LVIDs, LVPWd

Abbreviation: A2CH, apical 2-chamber; A4CH, apical 4-chamber; ED, end-diastole; ES, end-systole; HCM, hypertrophic cardiomyopathy; IVSs, systolic interventricular septum; LVIDs, systolic left ventricular internal dimension; LVPWd, diastolic left ventricular posterior wall; PLAX, parasternal long-axis, PSAX, parasternal short-axis at mid-level

Table 3.3 Echocardiography-Based Radiomic Features used in CA differentiation

	Radiomic Features
Conventional texture feature (F1), and %ΔF1	A2CH_ED_wavelet-HLH_glrlm_ShortRunHighGrayLevelEmphasis, ES_wavelet-HHH_glcm_SumSquares, wavelet-LHH_glcm_Autocorrelation, glszm_GrayLevelVariance, wavelet-LLH_glcm_Autocorrelation, rate_glrlm_LongRunHighGrayLevelEmphasis, wavelet-LLH_glrlm_RunLengthNonUniformity A4CH_ED_wavelet-HHH_firstorder_Uniformity, glcm_SumSquares, gldm_GrayLevelVariance, wavelet-LHL_firstorder_Mean, glcm_ JointAverage, ES_wavelet-HLH_glrlm_LongRunHighGrayLevel Emphasis, wavelet-LHH_glcm_JointAverage, wavelet-LHL_firstorder_Mean, glcm_ Autocorrelation, JointAverage, rate_firstorder_Kurtosis, glrlm_RunEntropy A4CH_rate_wavelet-LLL_firstorder_Kurtosis

	Gabor_A2CH_ES_glszm_LowGrayLevelZoneEmphasis, PSAX_ED_gldm_ SmallDependenceLowGrayLevelEmphasis, glszm_SmallAreaLowGray LevelEmphasis, A2CH_ED_glszm_SizeZoneNonUniformity, A4CH_ES_ glrlm_RunVariance, rate_firstorder_InterquartileRange, PLAX_ES_gldm_ DependenceVariance, PSAX_ES_glrlm_LowGrayLevelRunEmphasis, A2CH_ED_glcm_JointEnergy, A4CH_ES_glszm_SmallAreaLowGray LevelEmphasis, rate_glcm_JointEntropy, PLAX_rate_firstorder_Skewness, PSAX_ES_gldm_SmallDependenceLowGrayLevelEmphasis LoG_A2CH_ES_glrlm_LongRunHighGrayLevelEmphasis, A4CH_ES_glcm_JointAverage, rate_glszm_LowGrayLevelZoneEmphasis, PLAX_rate_firstorder_InterquartileRange, Uniformity, A4CH_ES_glcm_ Autocorrelation, ClusterShade, JointAverage, gldm_HighGrayLevel Emphasis, PLAX_rate_firstorder_90Percentile, A4CH_ED_firstorder_ Median, ES_glcm_Autocorrelation, PSAX_ED_glszm_SmallAreaHighGray LevelEmphasis, A4CH_ED_firstorder_Median, gldm_LargeDependence HighGrayLevelEmphasis, ES_glcm_Autocorrelation, glcm_JointAverage, gldm_HighGrayLevelEmphasis, LargeDependenceHighGrayLevelEmphasis PLAX_ED_glrlm_LongRunEmphasis, wavelet-HLH_glszm_GrayLevelNon Uniformity, wavelet-HLL_glrlm_RunLengthNonUniformity, ES_wavelet-LHH_glcm_Autocorrelation, wavelet-LHL_glcm_Autocorrelation PSAX_ES_wavelet-LHL_glcm_JointAverage, rate_wavelet-HHH_firstorder_Entropy
Harmonization-driven texture features (F2), and %ΔF2	A2CH_ED_firstorder_TotalEnergy, Entropy, Mean A4CH_ED_firstorder_TotalEnergy, Entropy, Mean, ES_glcm_JointEnergy, rate_firstorder_Kurtosis, MeanAbsoluteDeviation, RobustMeanAbsolute Deviation, RootMeanSquared, glcm_JointEnergy,

	glrlm_GrayLevelNonUniformity, glszm_GrayLevelNonUniformity, ngtdm_Coarseness PLAX_rate_gldm_LargeDependenceHighGrayLevelEmphasis
Myocardial shape (F3), and %ΔF3	A4CH_rate_MajorAxisLength PLAX_ED_MajorAxisLength, rate_Sphericity
Myocardial thickness (F4), and %ΔF4	ED_apexR, ES_apexR, rate_baseL, PLAX_LVIDd, LVPWd

Abbreviation: A2CH, apical 2-chamber; A4CH, apical 4-chamber; CA, cardiac amyloidosis; ED, end-diastole; ES, end-systole; LVIDd, diastolic left ventricular internal dimension LVPWd, diastolic left ventricular posterior wall; PLAX, parasternal long-axis, PSAX, parasternal short-axis at mid-level

Table 3.4 Echocardiography-Based Radiomic Features used in HHD differentiation

	Radiomic Features
Conventional texture feature (F1), and %ΔF1	Gabor_A4CH_ED_glcm_Idn LoG_A2CH_rate_glrlm_GrayLevelNonUniformity
Harmonization-driven texture features (F2), and %ΔF2	-
Myocardial shape (F3), and %ΔF3	A4CH_ED_Sphericity PLAX_ES_MajorAxisLength
Myocardial thickness (F4), and %ΔF4	PLAX_LVIDd, LVIDs

Abbreviation: A2CH, apical 2-chamber; A4CH, apical 4-chamber; ED, end-diastole; ES, end-systole; HHD, hypertensive heart disease; LVIDd, diastolic left ventricular internal dimension LVIDs, systolic left ventricular internal dimension; PLAX, parasternal long-axis

2.4.2. LVH Classification and Disease Discrimination Logic

Upon model detection of LVH from given subjects, our study imprints dedicated models to further classify and differentiate among three etiological conditions: HCM, CA, or HHD (Fig. 5A). Because the three classification models were not trained together, we could not derive the relative probabilities for HCM, CA, and HHD. Therefore, we applied the following logic to determine the classification results based on the results of the three models. The output probability values are binarized using the AUC threshold calculated by the Youden index.[29] When LVH was classified, there were eight possible scenarios because three binary classification models were applied (Table 4). If an LVH subject exhibits one of these three conditions exclusively, that condition is definitively classified as the etiology of LVH. For LVH subjects exhibiting two or more conditions, the model prioritizes the diagnosis associated with the highest probability, thereby assigning the most likely etiological classification. Furthermore, if the model could not select any of the three etiologies, it was categorized as "Others."

When LVH is detected without a positive indication for any of the specified three etiologies, the subject is categorized into an "Others" group. While it might seem natural to always make one of the three choices given that three diseases were used in modeling, echocardiography images alone may not always provide a precise diagnosis because of the nature of the disease. However, disease labeling is based on a combination of various types of clinical information, which may be difficult to discern from images alone. We believe that this ambiguity can be classified as "Others," demonstrating the scalability of our classification model. This designation suggests the presence of an alternative or unspecified LVH etiology not covered by the primary classifications of HCM, CA, or HHD.

2.4.3. Cardiac Cycle-Based Probability Mapping to Patient-Level Probability

We extracted features from the PLAX, PSAX, A4Ch, and A2Ch views. The data comprised videos of either 1 or 2 cardiac cycles. Our training data incorporated features synchronized across cardiac cycles from the four views. However, classification performance evaluation

must be performed at the patient level. Therefore, the probability values extracted per cardiac cycle must be converted into patient-level probabilities. Recent research has proposed the use of radiomics to build lesion-based models, suggesting transforming them into patient-level scores using an area under the curve (AUC) threshold.[30] We applied this technique to map the probabilities of diseases generated at the cardiac cycle level to the patient level.

The function transforms the probabilities per cycle within a patient by using the AUC threshold to determine the relative probability. It divides the probabilities into positive and negative based on a comparison of their magnitudes. Subsequently, the average is computed by adding an optimal threshold. This process maps patient-level probability from cycle-level probability.

Table 4. LVH disease decision-mapping logic

LVH	HCM	CA	HHD	Final Decision Mapping Logic
0				Normal
1	1	0	0	HCM
1	0	1	0	CA
1	0	0	1	HHD
1	1	0	1	Maximal probability between HCM vs. HHD
1	1	1	0	Maximal probability between HCM vs. CA
1	0	1	1	Maximal probability between CA vs. HHD
1	1	1	1	Maximal probability among HCM vs. CA vs. HHD
1	0	0	0	Others

Abbreviation: CA, cardiac amyloidosis; HCM, hypertrophic cardiomyopathy; HHD, hypertensive heart disease; LVH, left ventricular hypertrophy

2.5. Statistical Analysis

Categorical variables are presented as absolute counts and percentages, and continuous variables are expressed as means ± standard deviation or medians [interquartile range], as appropriate. Differences between categorical variables were analyzed using the chi-squared test or Fisher's exact test, as appropriate, while differences between continuous variables were assessed using the Student's t-test. For multiple comparisons, data were analyzed using one-way analysis of variance (ANOVA) or the Kruskal–Wallis method. Bonferroni correction was applied to reduce the possibility of Type I errors in multiple comparisons. The diagnostic performance was evaluated with the area under curve (AUC) sensitivity, specificity, and F1-score metrics. We employed Shapley Additive Explanations (SHAP) to gain insights into the predictions of machine learning (ML) models.[31] SHAP, a model-agnostic technique rooted in cooperative game theory that explains the influence of individual features and their values on the model's output. SHAP values were calculated by comparing the model predictions with and without the presence of features. In binary classification problems, a higher SHAP value indicates a higher probability of a positive class, whereas a lower SHAP value indicates a higher probability of a negative class. The importance of a feature was calculated by summing the absolute SHAP values of the features across all samples. For visualization with SHAP value, we selected one texture feature and extracted its feature map using Pyradiomics and extrated the SHAP values for each feature across all the validation data and normalized these values to calculate the relative SHAP values. The SHAP values of the selected features in each pixel, indicated by the feature map, were visualized on a color scale from green to orange (Fig. 6). A two-tailed p-value <0.05 was considered statistically significant. All analyses were performed using SAS version 9.4 (SAS Institute Inc., Cary, NC, USA) and R 3.3.0 (R Development Core Team, 2016).

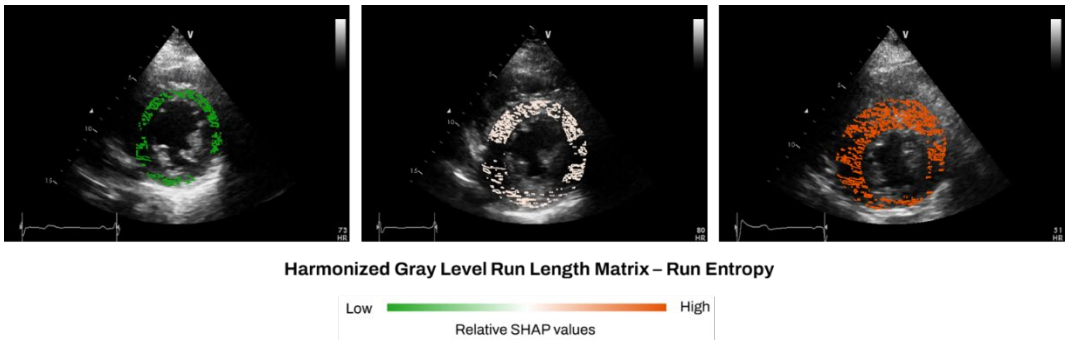

Fig. 7. Representative Cases of Feature Visuallization of Relative SHAP Values. Harmonized Gray Level Run Length Matrix—Run Entropy is a major feature in differentiating HCM etiology. The case presented on the left is a non-HCM case. The middle and right images show HCM. Because the model differentiates etiology by using multiple features in combination, the degree of the SHAP value of the feature may vary depending on the data.

Abbreviation: HCM, hypertrophic cardiomyopathy; SHAP, Shapley Additive Explanations.

3. RESULTS

3.1. Study Population

The developmental dataset comprised 867 patients (mean age, 52.0±17.9 years; 60.3% male). In this group, LVH was observed in 67.6% of the training set and 63.2% of the internal validation set, with no significant difference in the prevalence of LVH (P=0.323) or its etiologies (P=0.572) (Table 5). Age, proportion of men, body mass index also similar between both groups. The external validation set consisted of 619 patients (mean age, 51.3±14.6; 48.6% male) and showed a significantly lower proportion of men and LVH than the internal validation dataset (48.6% vs. 60.7%; P=0.008, 33.1% vs. 63.2%; P <0.001, respectively). In this cohort, HCM accounted for fewer cases (22.4% vs. 51.5%; P <0.001), while HHD was more common (45.4% vs. 20.4%; P <0.001). Comprehensive demographics and echocardiographic characteristics are provided in Table 6 and the subtype of HCM and CA are in Table 7.

3.2. LVH Detection

From the 19,839 features extracted for ML classification, 70 key features were utilized to detect LVH, achieving an AUC of 1.00 (95% confidence interval [CI], 1.00–1.00) in the internal validation (Fig. 7A). Similarly, the algorithm maintained an AUC of 1.00 (95% CI, 0.99-1.00) in the external validation in identifying LVH (Fig. 7B).

In the internal and external validation sets, patients identified as having LVH by the model showed smaller LV dimensions, thicker LV walls, and worsened LV diastolic function compared to normal subjects (Table 8). Notably, some normal subjects were misclassified as "Others" (1 in the internal and 6 in the external validation sets), having higher LV mass index (89.0 [82.8–102.8] vs. 74.1 [65.5–84.6] g/m2, P=0.002) and lower e' velocity (7.6 [6.9–9.0] vs. 10.4 [9.0–12.0] cm/s, P=0.006) than correctly classified as normal (Table 9).

Table 5. Baseline Characteristics of the Study Cohorts

	Developmental Set		External Validation	P-value[a]	P-value[b]
	Training (n=704)	Internal Validation (n=163)	(n=619)		
Age, years	52.1 ± 18.0	51.2 ± 17.3	51.3 ± 14.6	0.543	0.939
Men, n (%)	424 (60.2%)	99 (60.7%)	301 (48.6%)	0.975	0.008
BMI, kg/m2	23.8 ± 4.9	23.5 ± 3.8	23.9 ± 3.4	0.479	0.153
LVH, n (%)	476 (67.6%)	103 (63.2%)	205 (33.1%)	0.323	<0.001
HCM, n (%)	223 (46.8%)	53 (51.5%)	46 (22.4%)		
CA, n (%)	139 (29.2%)	29 (28.2%)	66 (32.2%)	0.572	<0.001
HHD, n (%)	114 (23.9%)	21 (20.4%)	93 (45.4%)		

Values are presented as mean ± SD or number (percentage).

[a] P-values were obtained using Student' s t-test or chi-squared analysis, comparing all patients across the training and internal validation sets.

[b] P-values were obtained using Student' s t-test or chi-squared analysis, comparing internal and external validation sets.

Abbreviation: BMI, body mass index; CA, cardiac amyloidosis; HCM, hypertrophic cardiomyopathy; HHD, hypertensive heart disease; LVH, left ventricular hypertrophy

Table 6.1 Detailed demographics and echocardiographic characteristics of the Study Cohorts

	Training			Internal Validation		
	Total (n = 704)	**Normal (n = 228)**	**LVH (n = 476)**	**Total (n = 163)**	**Normal (n = 60)**	**LVH (n = 103)**
Clinical Parameters						
Age, years	52.1 ± 18.0	35.4 ± 12.5	60.2 ± 14.3	51.2 ± 17.3	36.9 ± 12.3	59.5 ± 14.0
Men, n (%)	424 (60.2%)	101 (44.3%)	323 (67.9%)	99 (60.7%)	29 (48.3%)	70 (68.0%)
Height, cm	165.1 ±10.0	166.4 ± 8.3	164.5 ± 10.6	165.6 ± 8.8	166.4 ± 8.9	165.0 ± 8.8
Weight, kg	65.1 ± 13.5	61.5 ± 10.9	66.9 ± 14.2	64.9 ± 14.9	61.1 ± 10.8	67.1 ± 15.4
BMI, kg/m^2	23.8 ± 4.9	22.1 ± 2.8	24.7 ± 5.4	23.5 ± 3.8	21.9 ± 2.6	24.4 ± 4.1
BSA, m^2	1.7 ± 0.2	1.7 ± 0.2	1.7 ± 0.2	1.7 ± 0.2	1.7 ± 0.2	1.7 ± 0.2
SBP, mmHg	121.9 ± 19.8	116.8 ± 11.1	124.3 ± 22.3	120.3 ± 17.7	116.9 ± 12.0	122.3 ± 20.1
DBP, mmHg	74.4 ± 13.1	72.1 ± 9.6	75.5 ± 14.4	73.9 ± 12.4	72.5 ± 9.9	74.7 ± 13.6
Hypertension	264 (37.5%)	0 (0.0%)	264 (55.5%)	50 (30.7%)	0 (0.0%)	50 (48.5%)
Diabetes	91 (12.9%)	0 (0.0%)	91 (19.1%)	16 (9.8%)	0 (0.0%)	16 (15.5%)
Atrial fibrillation	55 (7.8%)	0 (0.0%)	55 (11.6%)	8 (4.9%)	0 (0.0%)	8 (10.4%)
Coronary artery disease	76 (10.8%)	0 (0.0%)	76 (16.0%)	10 (6.1%)	0 (0.0%)	10 (9.7%)
Chronic kidney disease	62 (8.8%)	0 (0.0%)	62 (17.0%)	11 (6.7%)	0 (0.0%)	11 (10.6%)
LVH Etiology						
HCM			223 (31.7%)			53 (32.5%)
CA			139 (19.7%)			29 (17.8%)
HHD			114 (16.2%)			21 (12.9%)
Echocardiographic parameter						
LVIDd, mm	42.1 ± 15.0	47.7 ± 3.8	39.4 ± 17.4	42.5 ± 14.8	47.9 ± 3.6	39.4 ± 17.8
LVIDs, mm	28.2 ± 10.4	31.2 ± 3.4	26.7 ± 12.2	28.1 ± 10.7	31.1 ± 2.9	26.4 ± 13.0
IVS, mm	11.0 ± 5.5	8.0 ± 1.1	12.5 ± 6.1	10.7 ± 3.9	8.1 ± 1.2	12.3 ± 5.9
LVPW, mm	9.4 ± 3.8	8.1 ± 1.0	10.0 ± 4.6	9.0 ± 3.7	8.1 ± 1.2	9.6 ± 4.5
LVEF, %	62.8 ±10.0	66.6 ± 4.9	60.9 ± 11.3	63.9 ± 10.0	67.3 ± 4.5	61.9 ± 11.7

LVMI, g/m^2	125.9 ± 51.2	76.1 ± 14.8	149.9 ± 44.8	119.0 ± 43.0	77.2 ± 14.9	143.6 ± 34.1
RWT	0.5 ± 0.1	0.3 ± 0.0	0.5 ± 0.1	0.4 ± 0.1	0.3 ± 0.1	0.5 ± 0.1
LA volume index, mL/m^2	39.6 ± 18.1	25.4 ± 5.3	46.4 ± 18.1	37.2 ± 16.1	25.2 ± 4.8	44.4 ± 16.2
E velocity, cm/s	76.6 ± 21.6	79.4 ± 14.5	74.8 ± 25.0	72.2 ± 20.8	78.3 ± 15.6	67.4 ± 23.1
A velocity, cm/s	58.3 ± 21.2	48.7 ± 10.5	65.3 ± 24.1	54.0 ± 17.8	48.4 ± 10.1	58.6 ± 21.2
e' velocity, cm/s	7.2 ± 3.8	11.4 ± 2.0	4.6 ± 1.8	7.5 ± 3.8	11.3 ± 2.0	4.5 ± 1.4
E/e'	14.3 ± 9.3	7.1 ± 1.5	17.8 ± 9.5	13.0 ± 8.1	7.0 ± 1.3	16.5 ± 8.4
RVSP, mmHg	28.4 ± 10.7	22.5 ± 3.8	31.8 ± 11.7	27.6 ± 9.3	22.9 ± 3.3	30.7 ± 10.7

Table 6.2 Detailed demographics and echocardiographic characteristics of the Study Cohorts

	External Validation			P-value*
	Total (n = 619)	**Normal (n = 414)**	**LVH (n = 205)**	
Clinical Parameters				
Age, years	51.3 ± 14.6	47.4 ± 12.0	59.1 ± 16.3	0.609
Men, n (%)	301 (48.6%)	184 (44.4%)	117 (57.1%)	<0.001
Height, cm	165.0 ± 9.3	165.2 ± 8.7	164.7 ± 10.5	0.829
Weight, kg	65.6 ± 12.8	64.1 ± 10.7	68.7 ± 15.8	0.735
BMI, kg/m^2	23.9 ± 3.4	23.4 ± 2.6	25.1 ± 4.4	0.491
BSA, m^2	1.7 ± 0.2	1.7 ± 0.2	1.8 ± 0.2	0.808
SBP, mmHg	127.6 ± 21.5	122.3 ± 13.5	138.9 ± 29.6	<0.001
DBP, mmHg	76.7 ± 14.9	73.8 ± 8.6	83.1 ± 22.0	0.004
Hypertension	113 (18.3%)	0 (0.0%)	113 (55.1%)	<0.001
Diabetes	39 (6.3%)	0 (0.0%)	39 (19.0%)	<0.001
Atrial fibrillation	17 (2.7%)	0 (0.0%)	17 (8.3%)	0.001
Coronary artery disease	7 (1.1%)	0 (0.0%)	7 (3.4%)	<0.001
Chronic kidney disease	12 (1.9%)	0 (0.0%)	12 (5.9%)	<0.001
Etiology of LVH				
HCM			46 (7.4%)	<0.001
CA			66 (10.7%)	

HHD			93 (15.0%)	
Echocardiographic parameter				
LVIDd, mm	46.0 ± 5.0	46.0 ± 3.8	45.9 ± 6.9	<0.001
LVIDs, mm	30.0 ± 5.1	29.5 ± 3.7	30.9 ± 7.0	<0.001
IVS, mm	10.7 ± 3.3	8.6 ± 1.2	15.1 ± 3.7	0.529
LVPW, mm	9.9 ± 2.8	8.4 ± 1.1	13.0 ± 2.6	0.004
LVEF, %	61.9 ± 6.9	63.6 ± 4.0	58.3 ± 9.6	0.021
LVMI, g/m^2	100.0 ± 43.0	75.0 ± 13.3	150.8 ± 37.4	<0.001
RWT	0.4 ± 0.1	0.4 ± 0.0	0.6 ± 0.1	0.002
LA volume index, mL/m^2	35.5 ± 15.4	28.6 ± 5.3	49.6 ± 19.1	<0.001
E velocity, cm/s	76.5 ± 19.6	75.9 ± 16.0	77.7 ± 25.7	0.068
A velocity, cm/s	62.3 ± 19.0	58.1 ± 13.6	71.9 ± 25.2	<0.001
e' velocity, cm/s	8.6 ± 3.3	10.3 ± 2.3	5.0 ± 1.9	<0.001
E/e'	11.0 ± 8.2	7.6 ± 1.8	18.2 ± 11.2	<0.001
RVSP, mmHg	26.9 ± 8.1	24.3 ± 4.3	32.6 ± 11.0	0.032

Values are presented as mean ± SD or numbers (percentages).

* P-values were obtained through analysis of variance (ANOVA) or chi-square analysis, comparing all patients across the training, validation, and external validation cohorts.

Abbreviations: BMI, body mass index; BSA, body surface area; CA, cardiac amyloidosis; DBP, diastolic blood pressure; HCM, hypertrophic cardiomyopathy; HHD, hypertensive heart disease; IVS, interventricular septum; LA, left atrial; LVEF, left ventricular ejection fraction; LVH, left ventricular hypertrophy; LVIDd, diastolic left ventricular internal dimension; LVIDs, systolic left ventricular internal dimension; LVMI, left ventricular mass index; LVPW, left ventricular posterior wall; RVSP, right ventricular systolic pressure; RWT, relative wall thickness; SBP, systolic blood pressure.

Table 7. Subtype of HCM and CA of the study cohort

	Developmental Set			External Test	P-value[a]	P-value[b]
	Total	Training	Internal Validation			
HCM	(n=276)	(n=223)	(n=53)	(n=46)		
Apical, n (%)	35 (12.7%)	25 (12.7%)	10 (18.9%)	3 (6.5%)		
Septal, n (%)	145 (52.5%)	117 (52.5%)	28 (52.8%)	10 (21.7%)	0.250	<0.001
Mixed or diffuse, n (%)	96 (34.8%)	81 (36.3%)	15 (28.3%)	33 (71.7%)		
CA	(n=168)	(n=139)	(n=29)	(n=66)		
AL, n (%)	142 (84.5%)	115 (82.7%)	27 (93.1%)	59 (89.4%)		
ATTR, n (%)	17 (10.1%)	16 (11.5%)	1 (3.4%)	7 (10.6%)	0.353	0.159
AA, n (%)	9 (5.4%)	8 (5.8%)	1 (3.4%)	-		

Values are presented as number (percentage).

[a] P-values were obtained using chi-squared analysis, comparing patients across the training and internal validation sets.

[b] P-values were obtained using chi-squared analysis, comparing developmental and external test sets.

Abbreviation: AA, amyloid A; AL, amyloid light-chain; ATTR, amyloid transthyretin; CA, cardiac amyloidosis; HCM, hypertrophic cardiomyopathy

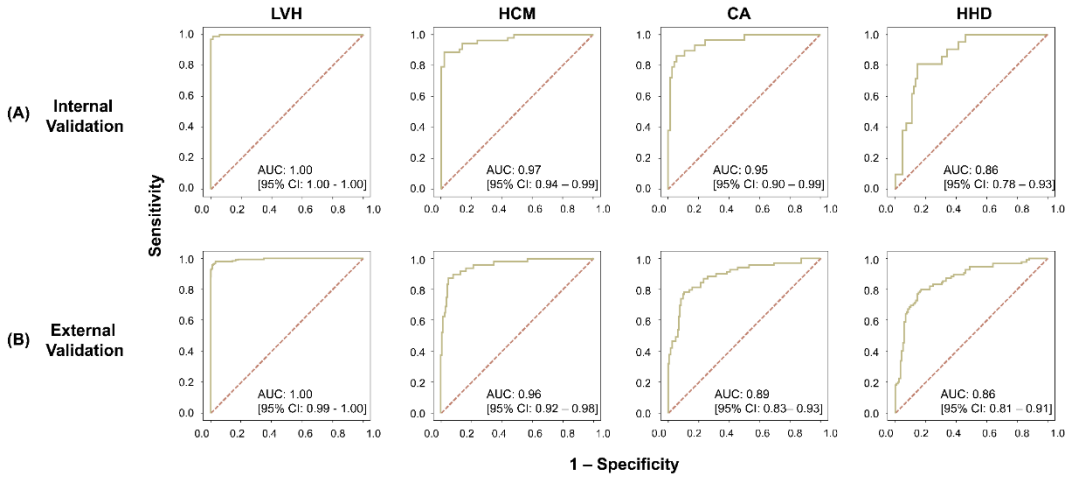

Fig. 8. Performance of the ML Classification Model in Differentiating the Etiology of LVH.
The AUC illustrates the diagnostic performance of the ML classification model for the detection of LVH and for the differentiation of HCM, CA, and HHD from other causes of LVH in both (A) the internal validation cohort and (B) the external validation cohort.
Abbreviations: AUC, area under the curve; CA, cardiac amyloidosis; CI, confidence interval; HCM, hypertrophic cardiomyopathy; HHD, hypertensive heart disease; LVH, left ventricular hypertrophy

Table 8.1 Group-Based Patient Baseline Characteristics as Classified by the Integrated ML Model Across the Validation Sets

	Normal (n = 469)	LVH (n = 313)	P-value
Clinical Parameters			
Age, years	46.1 ± 12.6	59.1 ± 15.5	<0.001
Men, n (%)	208 (44.3%)	1922(61.3%)	<0.001
Height, cm	165.3 ± 8.8	164.9 ± 9.9	0.476
Weight, kg	63.7 ± 10.8	68.1 ± 15.5	<0.001
BMI, kg/m^2	23.2 ± 2.7	24.9 ± 4.3	<0.001
BSA, m^2	1.7 ± 0.2	1.8 ± 0.2	0.001
SBP, mmHg	121.6 ± 13.4	133.0 ± 27.7	<0.001
DBP, mmHg	73.6 ± 8.7	80.2 ± 19.8	<0.001
Hypertension	0 (0.0%)	163 (52.1%)	<0.001
Diabetes	1 (0.2%)	54 (17.3%)	<0.001
Atrial fibrillation	0 (0.0%)	25 (8.0%)	<0.001
Coronary artery disease	0 (0.0%)	17 (5.4%)	<0.001
Chronic kidney disease	0 (0.0%)	23 (7.3%)	<0.001
Echocardiographic Parameters			
LVIDd, mm	46.2 ± 4.3	43.9 ± 11.7	0.001
LVIDs, mm	29.7 ± 3.9	29.4 ± 9.4	0.625
IVS, mm	8.5 ± 1.2	14.1 ± 4.7	<0.001
LVPW, mm	8.3 ± 1.1	11.9 ± 3.7	<0.001
LVEF, %	64.0 ± 4.3	59.7 ± 10.4	<0.001
LVMI, g/m^2	75.4 ± 14.5	147.0 ± 37.1	<0.001
RWT	0.4 ± 0.1	0.5 ± 0.1	<0.001
LA volume index, mL/m^2	28.2 ± 5.6	47.4 ± 18.4	<0.001
E velocity, cm/s	76.3 ± 16.0	74.7 ± 25.2	0.349
A velocity, cm/s	56.8 ± 13.7	67.9 ± 24.6	<0.001
e' velocity, cm/s	10.5 ± 2.3	4.9 ± 1.9	<0.001
E/e'	7.5 ± 1.7	17.4 ± 10.4	<0.001

RVSP, mmHg	24.1 ± 4.1	31.7 ± 10.9	<0.001

Table 8.2 Group-Based Patient Baseline Characteristics as Classified by the Integrated ML Model Across the Validation Sets

	HCM (n = 94)	CA (n = 87)	HHD (n = 97)	P-value*
Clinical Parameters				
Age, years	58.6 ± 14.0‡	67.6 ± 13.3‡	52.2 ± 15.2‡	<0.001
Men, n (%)	47 (50.0%)†	47 (54.0%)†	76 (78.4%)‡	<0.001
Height, cm	164.4 ± 10.7†	164.4 ± 10.7†	167.9 ± 8.1‡	<0.001
Weight, kg	69.3 ± 13.0†	59.5 ± 13.1‡	74.2 ± 15.8†	<0.001
BMI, kg/m^2	25.6 ± 4.0†	22.7 ± 3.2‡	26.2 ± 4.6†	<0.001
BSA, m^2	1.8 ± 0.2‡	1.6 ± 0.2‡	1.9 ± 0.2‡	<0.001
SBP, mmHg	127.6 ± 22.3‡	118.5 ± 22.9‡	149.6 ± 26.6‡	<0.001
DBP, mmHg	74.7 ± 13.9†	72.7 ± 15.1†	90.0 ± 13.9‡	<0.001
Hypertension	31 (33.0%)†	33 (37.9%)†	77 (79.4%)‡	<0.001
Diabetes	13 (13.8%)	13 (14.9%)	18 (18.6%)	0.878
Atrial fibrillation	6 (6.4%)	13 (14.9%)†	2 (2.1%)†	0.003
Coronary artery disease	5 (5.3%)	4 (4.6%)	5 (5.2%)	0.918
Chronic kidney disease	3 (3.2%)	11 (12.6%)	7 (7.2%)	0.072
Echocardiographic Parameters				
LVIDd, mm	40.7 ± 14.1†	42.2 ± 9.9†	48.4 ± 10.3‡	<0.001
LVIDs, mm	24.4 ± 8.9‡	30.7 ± 9.2†	33.4 ± 8.9†	<0.001
IVS, mm	15.8 ± 6.5‡	13.6 ± 3.4†	13.2 ± 3.4†	<0.001
LVPW, mm	10.1 ± 4.0‡	13.1 ± 3.3†	12.4 ± 3.0†	<0.001
LVEF, %	66.4 ± 7.6‡	54.1 ± 11.0†	57.2 ± 9.5†	<0.001
LVMI, g/m^2	153.4 ± 34.4	145.2 ± 42.3	149.4 ± 33.9	0.331
RWT	0.5 ± 0.1†	0.6 ± 0.2‡	0.5 ± 0.1†	<0.001
LA volume index, mL/m^2	49.4 ± 19.7†	53.6 ± 17.0†	42.6 ± 16.9‡	<0.001
E velocity, cm/s	65.3 ± 19.8†	89.5 ± 26.3‡	71.0 ± 24.0†	<0.001
A velocity, cm/s	65.0 ± 22.1†	60.3 ± 28.6†	75.2 ± 20.8‡	<0.001

e' velocity, cm/s	4.5 ± 1.4†	4.0 ± 1.5†	5.8 ± 1.9‡	<0.001
E/e'	15.6 ± 7.8‡	24.9 ± 12.4‡	12.9 ± 4.8‡	<0.001
RVSP, mmHg	29.6 ± 8.4†	37.6 ± 12.4‡	28.8 ± 9.6†	<0.001

Values are presented as mean ± SD or numbers (percentages).

* P-values were obtained through analysis of variance (ANOVA) or chi-square analysis, comparing multiple groups.

†Statistically different from the other two groups. ‡Statistically different from both other groups after Bonferroni correction.

Abbreviations: BMI, body mass index; BSA, body surface area; CA, cardiac amyloidosis; DBP, diastolic blood pressure; HCM, hypertrophic cardiomyopathy; HHD, hypertensive heart disease; IVS, interventricular septum; LA, left atrial; LVEF, left ventricular ejection fraction; LVH, left ventricular hypertrophy; LVIDd, diastolic left ventricular internal dimension; LVIDs, systolic left ventricular internal dimension; LVMI, left ventricular mass index; LVPW, left ventricular posterior wall; ML, machine-learning; RVSP, right ventricular systolic pressure; RWT, relative wall thickness; SBP, systolic blood pressure.

Table 9. Comparison Between Correctly Classified Subjects to Those Misclassified as "Others" in the Normal Group

	Normal (n = 467)	Others (n = 7)	P-value
Clinical Parameters			
Age, years	47.0 [37.0 – 55.0]	52.1 [49.2 – 60.3]	0.128
Men, n (%)	207 (44.3%)	6 (85.7%)	0.071
Height, cm	164.0 [159.1 – 172.0]	168.0 [166.0 – 171.8]	0.250
Weight, kg	63.0 [56.0 – 71.0]	70.5 [67.0 – 77.5]	0.050
BMI, kg/m^2	23.2 [21.2 – 25.2]	24.8 [23.8 – 25.4]	0.120
BSA, m^2	1.7 [1.6 – 1.8]	1.8 [1.8 – 2.0]	0.061
SBP, mmHg	121.0 [112.0 – 129.0]	137.0 [111.0 – 138.0]	0.321
DBP, mmHg	74.0 [68.0 – 79.0]	80.0 [73.5 – 86.0]	0.134
Hypertension	0 (0.0%)	0 (0.0%)	
Diabetes	0 (0.0%)	0 (0.0%)	
Atrial fibrillation	0 (0.0%)	0 (0.0%)	
Coronary artery disease	0 (0.0%)	0 (0.0%)	
Chronic kidney disease	0 (0.0%)	0 (0.0%)	
Echocardiographic Parameter			
LVIDd, mm	46.0 [44.0 – 49.0]	49.0 [46.0 – 51.0]	0.206
LVIDs, mm	30.0 [27.0 – 32.0]	28.0 [26.5 – 31.0]	0.390
IVS, mm	8.0 [8.0 – 9.0]	10.0 [9.0 – 11.0]	0.002
LVPW, mm	8.0 [8.0 – 9.0]	10.0 [9.0 – 10.0]	0.001
LVEF, %	64.0 [61.0 – 66.9]	65.0 [60.4 – 69.1]	0.768
LVMI, g/m^2	74.1 [65.5 – 84.6]	89.0 [82.8 – 102.8]	0.002
RWT	0.4 [0.3 – 0.4]	0.4 [0.4 – 0.4]	0.022
LA volume index, mL/m^2	28.1 [24.3 – 31.7]	31.6 [27.0 – 33.0]	0.216
E velocity, cm/s	75.0 [65.0 – 86.0]	72.0 [61.0 – 75.0]	0.298
A velocity, cm/s	56.0 [46.0 – 66.0]	64.0 [57.5 – 68.0]	0.113
e' velocity, cm/s	10.4 [9.0 – 12.0]	7.6 [6.9 – 9.0]	0.006
E/e'	7.2 [6.3 – 8.4]	8.4 [7.0 – 10.4]	0.159

RVSP, mmHg	24.0 [21.0 – 26.2]	22.7 [21.0 – 24.4]	0.377

Values are presented as mean ± SD, medians [interquartile ranges], or numbers (percentages).
Abbreviations: BMI, body mass index; BSA, body surface area; CA, cardiac amyloidosis; DBP, diastolic blood pressure; HCM, hypertrophic cardiomyopathy; HHD, hypertensive heart disease; IVS, interventricular septum; LA, left atrial; LVEF, left ventricular ejection fraction; LVIDd, diastolic left ventricular internal dimension; LVIDs, systolic left ventricular internal dimension; LVMI, left ventricular mass index; LVPW, left ventricular posterior wall; RVSP, right ventricular systolic pressure; RWT, relative wall thickness; SBP, systolic blood pressure.

3.3. LVH Etiology Differentiation

To differentiate LVH etiology, our ML model utilized selected features for each condition: 82 for HCM, 83 for CA, and six for HHD. In the internal validation set, the model predicted HCM with an AUC of 0.97 (95% CI, 0.94–0.99). For CA and HHD, AUCs were 0.95 (0.90–0.99) and 0.86 (0.78–0.93), respectively (Table 10). ROC curves are provided in Fig. 8A. The external validation set showed consistent performance with comparable AUCs of 0.96 (0.92–0.98) for HCM, 0.89 (0.83–0.93) for CA, and 0.86 (0.81–0.91) for HHD (Fig. 8B). The overall accuracy of the multi-class classification reached 89.0% in the internal validation set and 92.4% in the external validation set (Fig. 6B and C).

When comparing the clinical and echocardiographic parameters across groups classified by our model as HCM, CA, and HHD, no significant differences in LV mass index were observed (Table 8). Subjects predicted as HCM had smaller LV dimensions and the highest LV ejection fraction (LVEF), whereas those predicted as CA displayed the lowest LVEF and the worst LV diastolic function. Altogether, 28 LVH patients were misclassified into "Others" across both validation sets (four and two patients with HCM, three and six with CA, and three and 10 with HHD in the internal and external validation sets, respectively). Patients with misclassified HCM exhibited higher diastolic blood pressure and lower LVEF compared to those correctly classified (Table 11). For CA, misclassified patients more often had diabetes mellitus and higher LVEF (Table 12). In the case of HHD, misclassified patients showed smaller LV cavities and higher LVEF (Table 13).

Table 10. Diagnostic Performance of Echocardiographic Feature Model for Distinguishing LVH Etiology in Internal and External Validation Datasets

	Sensitivity	Specificity	F1	PPV	NPV
Internal validation					
LVH	0.98	0.99	0.98	0.98	0.99
HCM	0.87	1.00	0.93	1.00	0.94
CA	0.83	0.99	0.87	0.92	0.96
HHD	0.76	0.97	0.78	0.80	0.97
External validation					
LVH	0.98	1.00	0.99	1.00	0.97
HCM	0.89	0.99	0.87	0.85	0.99
CA	0.80	0.97	0.84	0.87	0.98
HHD	0.75	0.99	0.82	0.91	0.96

Abbreviation: CA, cardiac amyloidosis; HCM, hypertrophic cardiomyopathy; HHD, hypertensive heart disease; LVH, left ventricular hypertrophy; NPV, negative predictive value; PPV, positive predictive value.

Table 11. Comparison Between Correctly Classified Subjects to Those Misclassified as "Others" in the HCM Group

	HCM		
	Classified Correctly (n = 87)	**Others (n = 6)**	**P-value**
Clinical Parameters			
Age, years	60.2 [49.0 – 68.0]	53.8 [45.3 – 57.0]	0.274
Men, n (%)	40 (46.0%)	3 (50.0%)	>0.999
Height, cm	165.0 [158.0 – 172.0]	167.5 [163.0 – 171.0]	0.439
Weight, kg	69.0 [60.5 – 77.5]	70.8 [61.0 – 76.0]	0.839
BMI, kg/m^2	24.9 [23.0 – 27.5]	24.5 [22.7 – 27.4]	0.667
BSA, m^2	1.8 [1.6 – 1.9]	1.8 [1.7 – 1.9]	0.845
SBP, mmHg	126.0 [113.0 – 138.0]	134.0 [132.0 – 148.0]	0.222
DBP, mmHg	74.0 [66.0 – 81.5]	86.0 [85.0 – 91.0]	0.034
Hypertension	29 (33.3%)	5 (83.3%)	0.106
Diabetes	12 (13.8%)	0 (0.0%)	0.618
Atrial fibrillation	6 (6.9%)	1 (16.7%)	>0.999
Coronary artery disease	5 (5.7%)	0 (0.0%)	>0.999
Chronic kidney disease	3 (3.4%)	0 (0.0%)	>0.999
Echocardiographic parameter			
LVIDd, mm	45.0 [40.0 – 48.0]	49.0 [37.0 – 50.0]	0.462
LVIDs, mm	26.0 [22.0 – 29.1]	30.5 [25.0 – 35.0]	0.199
IVS, mm	16.0 [14.0 – 20.0]	15.5 [9.0 – 20.0]	0.451
LVPW, mm	10.0 [9.0 – 12.0]	8.5 [6.0 – 11.0]	0.302
LVEF, %	67.6 [63.8 – 70.8]	61.2 [61.0 – 63.0]	0.013
LVMI, g/m^2	156.1 [127.4 – 171.6]	126.8 [119.8 – 150.5]	0.076
RWT	0.5 [0.4 – 0.5]	0.4 [0.3 – 0.4]	0.171
LA volume index, mL/m^2	46.0 [36.7 – 57.7]	40.1 [31.2 – 46.1]	0.252
E velocity, cm/s	60.5 [50.1 – 77.0]	40.1 [31.2 – 46.1]	0.954
A velocity, cm/s	57.0 [48.0 – 78.7]	57.9 [44.0 – 70.0]	0.418
e' velocity, cm/s	4.4 [3.5 – 5.3]	4.9 [4.3 – 5.1]	0.293

E/e'	13.8 [10.4 – 19.8]	14.4 [9.0 – 15.0]	0.579
RVSP, mmHg	29.4 [23.9 – 34.0]	27.0 [25.6 – 28.0]	0.921

Values are presented as medians [interquartile ranges] or numbers (percentages).

Abbreviations: BMI, body mass index; BSA, body surface area; CA, cardiac amyloidosis; DBP, diastolic blood pressure; HCM, hypertrophic cardiomyopathy; HHD, hypertensive heart disease; IVS, interventricular septum; LA, left atrial; LVEF, left ventricular ejection fraction; LVIDd, diastolic left ventricular internal dimension; LVIDs, systolic left ventricular internal dimension; LVMI, left ventricular mass index; LVPW, left ventricular posterior wall; RVSP, right ventricular systolic pressure; RWT, relative wall thickness; SBP, systolic blood pressure.

Table 12. Comparison Between Correctly Classified Subjects to Those Misclassified as "Others" in the CA Group

	CA		
	Classified Correctly (n = 77)	**Others (n = 9)**	**P-value**
Clinical Parameters			
Age, years	70.2 [65.0 – 77.9]	76.0 [57.0 – 81.0]	0.489
Men, n (%)	39 (50.6%)	6 (66.7%)	0.528
Height, cm	162.0 [152.0 – 167.3]	157.0 [154.4 – 162.9]	0.621
Weight, kg	58.0 [49.0 – 65.2]	56.0 [50.2 – 72.0]	0.860
BMI, kg/m^2	22.0 [20.3 – 24.7]	23.8 [22.3 – 25.6]	0.323
BSA, m^2	1.6 [1.5 – 1.7]	1.5 [1.4 – 1.8]	0.983
SBP, mmHg	113.0 [100.5 – 127.0]	115.0 [11.0 – 117.0]	0.921
DBP, mmHg	69.0 [63.5 – 75.5]	70.0 [61.0 – 71.0]	0.442
Hypertension	24 (31.2%)	4 (44.4%)	0.625
Diabetes	13 (16.9%)	5 (55.6%)	0.019
Atrial fibrillation	12 (15.6%)	2 (22.2%)	0.950
Coronary artery disease	4 (5.2%)	2 (22.2%)	0.215
Chronic kidney disease	10 (13.0%)	2 (22.2%)	0.781
Echocardiographic parameter			
LVIDd, mm	42.0 [39.0 – 45.0]	39.0 [36.0 – 43.0]	0.210
LVIDs, mm	29.0 [26.0 – 34.0]	28.0 [21.0 – 30.0]	0.167
IVS, mm	14.0 [12.0 – 16.0]	15.0 [13.0 – 16.0]	0.239
LVPW, mm	12.2 [11.0 – 15.2]	15.0 [12.0 – 16.0]	0.279
LVEF, %	56.8 [49.8 – 61.1]	60.2 [58.3 – 64.0]	0.046
LVMI, g/m^2	134.3 [106.9 – 161.0]	147.2 [117.0 – 167.4]	0.892
RWT	0.6 [0.5 – 0.7]	0.7 [0.6 – 0.8]	0.070
LA volume index, mL/m^2	51.5 [43.8 – 59.8]	45.6 [36.5 – 47.2]	0.122
E velocity, cm/s	90.0 [70.0 – 110.5]	81.2 [74.0 – 97.0]	0.623
A velocity, cm/s	59.0 [36.0 – 79.0]	70.9 [38.0 – 84.0]	0.675
e' velocity, cm/s	3.8 [3.0 – 4.5]	3.5 [2.5 – 4.0]	0.264

E/e'	23.1 [17.9 – 30.7]	21.8 [19.3 – 27.1]	0.959
RVSP, mmHg	36.4 [30.0 – 47.4]	34.2 [29.0 – 42.1]	0.506

Values are presented as medians [interquartile ranges] or numbers (percentages).

Abbreviations: BMI, body mass index; BSA, body surface area; CA, cardiac amyloidosis; DBP, diastolic blood pressure; HCM, hypertrophic cardiomyopathy; HHD, hypertensive heart disease; IVS, interventricular septum; LA, left atrial; LVEF, left ventricular ejection fraction; LVIDd, diastolic left ventricular internal dimension; LVIDs, systolic left ventricular internal dimension; LVMI, left ventricular mass index; LVPW, left ventricular posterior wall; RVSP, right ventricular systolic pressure; RWT, relative wall thickness; SBP, systolic blood pressure.

Table 13. Comparison Between Correctly Classified Subjects to Those Misclassified as "Others" in the HHD Group

	HHD		
	Classified Correctly (n = 86)	**Others (n = 13)**	**P-value**
Clinical Parameters			
Age, years	47.7 [40.0 – 58.0]	49.0 [45.0 – 57.0]	0.354
Men, n (%)	69 (80.2%)	10 (76.9%)	>0.999
Height, cm	170.0 [165.0 – 173.0]	170.0 [167.0 – 177.0]	0.705
Weight, kg	75.2 [64.0 – 85.3]	70.0 [66.3 – 89.0]	0.740
BMI, kg/m^2	26.0 [22.8 – 29.2]	25.1 [23.2 – 28.4]	0.569
BSA, m^2	1.9 ± 0.2	1.9 ± 0.3	0.933
SBP, mmHg	154.1 ± 24.7	160.0 ± 33.1	0.466
DBP, mmHg	90.0 [79.5 – 105.5]	102.5 [87.5 – 116.5]	0.168
Hypertension	74 (86.0%)	13 (100.0%)	0.327
Diabetes	17 (19.8%)	5 (38.5%)	0.249
Atrial fibrillation	1 (1.2%)	1 (7.7%)	0.616
Coronary artery disease	5 (5.8%)	1 (7.7%)	>0.999
Chronic kidney disease	6 (7.0%)	0 (0.0%)	0.720
Echocardiographic parameter			
LVIDd, mm	50.0 [47.0 – 54.0]	47.0 [45.0 – 49.0]	0.034
LVIDs, mm	35.0 [30.3 – 39.3]	30.0 [27.0 – 33.4]	0.044
IVS, mm	13.0 [12.0 – 15.0]	13.4 [13.0 – 15.0]	0.165
LVPW, mm	12.1 [12.0 – 14.0]	13.0 [12.0 – 14.0]	0.348
LVEF, %	58.0 [51.5 – 63.3]	62.4 [60.5 – 68.0]	0.013
LVMI, g/m^2	145.1 [125.6 – 171.6]	137.4 [126.6 – 144.4]	0.359
RWT	0.5 [0.5 – 0.5]	0.6 [0.5 – 0.6]	0.057
LA volume index, mL/m^2	37.5 [31.2 – 49.1]	37.9 [32.8 – 47.0]	0.950
E velocity, cm/s	65.0 [52.0 – 84.0]	58.5 [49.5 – 80.5]	0.446
A velocity, cm/s	76.8 ± 20.7	89.2 ± 23.0	0.070
e' velocity, cm/s	5.6 [4.6 – 6.7]	5.3 [3.0 – 6.8]	0.310

E/e'	11.1 [9.7 – 15.1]	11.9 [10.0 – 16.7]	0.495
RVSP, mmHg	26.2 [22.6 – 32.5]	25.3 [18.3 – 30.5]	0.452

Values are presented as the mean ± SD, median [interquartile range], or numbers (percentages).
Abbreviations: BMI, body mass index; BSA, body surface area; CA, cardiac amyloidosis; DBP, diastolic blood pressure; HCM, hypertrophic cardiomyopathy; HHD, hypertensive heart disease; IVS, interventricular septum; LA, left atrial; LVEF, left ventricular ejection fraction; LVIDd, diastolic left ventricular internal dimension; LVIDs, systolic left ventricular internal dimension; LVMI, left ventricular mass index; LVPW, left ventricular posterior wall; RVSP, right ventricular systolic pressure; RWT, relative wall thickness; SBP, systolic blood pressure.

3.4. Model Performances Comparing with Conventional Echocardiography

We evaluated the performance of various classification models, including two types of logistic regression; one using conventional echocardiographic parameters (LV ejection fraction, LV mass index, left atrial volume index, and E/e') and another using radiomic features. Among these, the LightGBM model demonstrated the best overall performance in distinguishing LVH etiology and was selected as the final model for the study. When compared with conventional echocardiographic parameters (Table 13), the final model demonstrated superior sensitivity (0.89 vs. 0.80 for HCM, 0.80 vs. 0.80 for CA, and 0.75 vs. 0.33 for HHD) and F1-score (0.87 vs. 0.57 for HCM, 0.84 vs. 0.72 for CA, and 0.82 vs. 0.50 for HHD).

3.5. Model Interpretation by SHAP Analysis in Assessing LVH

We analyzed SHAP values to identify key features influencing each classification model (Fig. 9). In distinguishing LVH from total subjects, harmonization-driven textures (F2), myocardial thickness (F4), and myocardial shape (F3) were pivotal. The total energy feature, derived via harmonization filtering and representing the sum of signal intensity across the myocardial area, emerged as the most critical factor in differentiating LVH. Key features for identifying HCM included harmonization-driven textures (F2), myocardial thickness (F4), and conventional textures (F1). Notably, run entropy from a gray-level run length matrix (GLRLM) after harmonization filtering was pivotal, quantifying uncertainty in matrix distribution to highlight texture heterogeneity. In detecting CA, our analysis identified conventional textures (F1), myocardial thickness (F4), and percent changes in myocardial thickness ([%Δ] F3) and harmonization-driven textures ([%Δ] F2) as key factors. Run Length Non-Uniformity with GLRLM stood out, measuring homogeneity across myocardial run lengths, with a lower value indicating greater homogeneity. Lastly, myocardial thickness (F4) and shape (F3) emerged as key determinants for HHD differentiation. The most crucial texture feature for HHD identified was the inverse difference normalized with the Gray Level Co-occurrence Matrix (GLCM), which measures the local homogeneity of the myocardial area. The comprehensive SHAP value analysis is summarized in Fig. 10.

We also analyzed SHAP values in cases misclassified as "Others" to understand the reasons for misclassification. By mapping the sum of SHAP values for texture features (F1 and F2) onto the myocardium, we found that properly classified cases exhibited considerably high SHAP values (Fig. 8), in contrast to the notably low SHAP values in misclassified "Others" cases (Fig. 10). This variance in myocardial texture features could have influenced the model's decision, indicating that these cases were divergent from their actual condition.

Table 14. Performance Comparison of Conventional and Radiomics-Based ML Model in the External Test Datasets

	Sensitivity	Specificity	F1-score	PPV	NPV
LVH					
Logistic Regression					
LVMI+LVEF	0.97	**1.00**	0.98	**1.00**	0.98
LVMI+LVEF+LAVI	0.97	**1.00**	0.98	**1.00**	0.98
LVMI+LVEF+LAVI+E/e'	**1.00**	**1.00**	**1.00**	**1.00**	**1.00**
Radiomics Features	0.98	**1.00**	0.99	**1.00**	0.99
LightGBM					
Radiomics Features	0.98	0.99	0.98	0.98	0.99
HCM					
Logistic Regression					
LVMI+LVEF	0.81	0.86	0.78	0.74	0.91
LVMI+LVEF+LAVI	0.77	0.86	0.75	0.73	0.89
LVMI+LVEF+LAVI+E/e'	0.74	0.93	0.78	0.83	0.88
Radiomics Features	0.75	0.98	0.84	0.95	0.89
LightGBM					
Radiomics Features	**0.87**	**1.00**	**0.93**	**1.00**	**0.94**
CA					
Logistic Regression					
LVMI+LVEF	0.76	0.88	0.66	0.58	0.94
LVMI+LVEF+LAVI	0.79	0.85	0.64	0.54	0.95
LVMI+LVEF+LAVI+E/e'	0.76	**0.99**	0.83	**0.92**	0.95
Radiomics Features	**0.83**	0.97	0.84	0.86	**0.96**
LightGBM					
Radiomics Features	**0.83**	**0.99**	**0.87**	**0.92**	**0.96**
HHD					
Logistic Regression					
LVMI+LVEF	0.10	**0.99**	0.17	0.67	0.88
LVMI+LVEF+LAVI	0.14	**0.99**	0.24	0.75	0.89

LVMI+LVEF+LAVI+E/e'	0.43	0.92	0.43	0.43	0.92
Radiomics Features	0.67	0.95	0.67	0.67	0.95
LightGBM					
Radiomics Features	**0.76**	0.97	**0.78**	**0.80**	**0.97**

Abbreviation; CA, cardiac amyloidosis; HCM, hypertrophic cardiomyopathy; HHD, hypertensive heart disease; LAVI, left atrial volume index; LVEF, left ventricular ejection fraction; LVH, left ventricular hypertrophy; LVMI, left ventricular mass index; NPV, negative predictive value; PPV, positive predictive value.

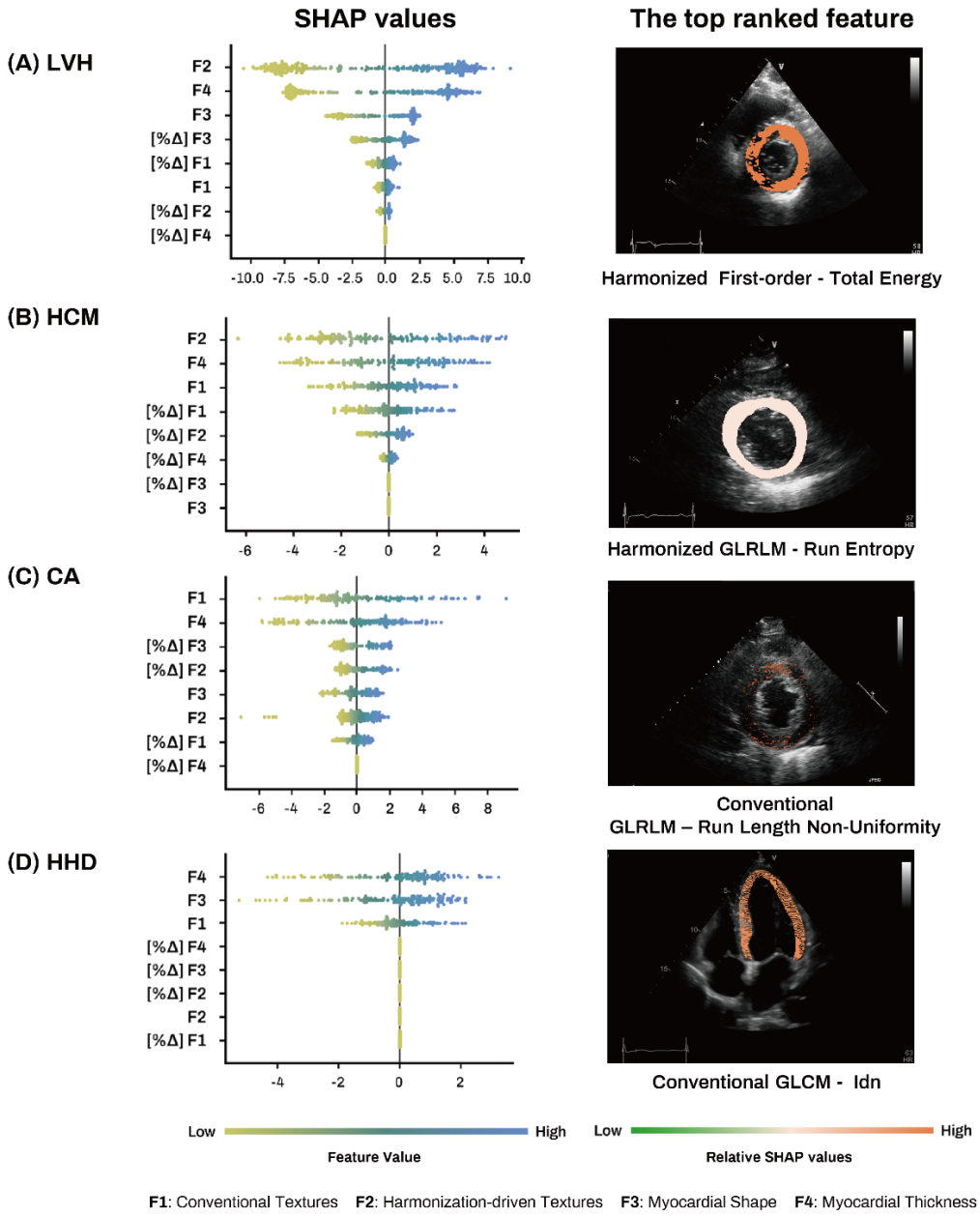

Fig. 9. Insights from SHAP Values and Feature Contribution in Classification Models. We employed SHAP values to the influence of features on the predictions made by classification models. Higher absolute SHAP values indicate a greater impact of belonging to the positive or

negative class. We performed the analysis through the whole classification process (A to D). The left panels depict feature contributions across the various integrated classification models. The right panels display representative mappings of the top-ranked features from both conventional (F1) and harmonization-driven (F2) texture analyses for each classified group, visualizing the differential impact of these features in the models.

Abbreviations: CA, cardiac amyloidosis; GLCM, Gray Level Co-occurrence Matrix; GLRLM, run entropy derived from a gray-level run length matrix; HCM, hypertrophic cardiomyopathy; HHD, hypertensive heart disease; LVH, left ventricular hypertrophy; SHAP, Shapley Additive Explanations.

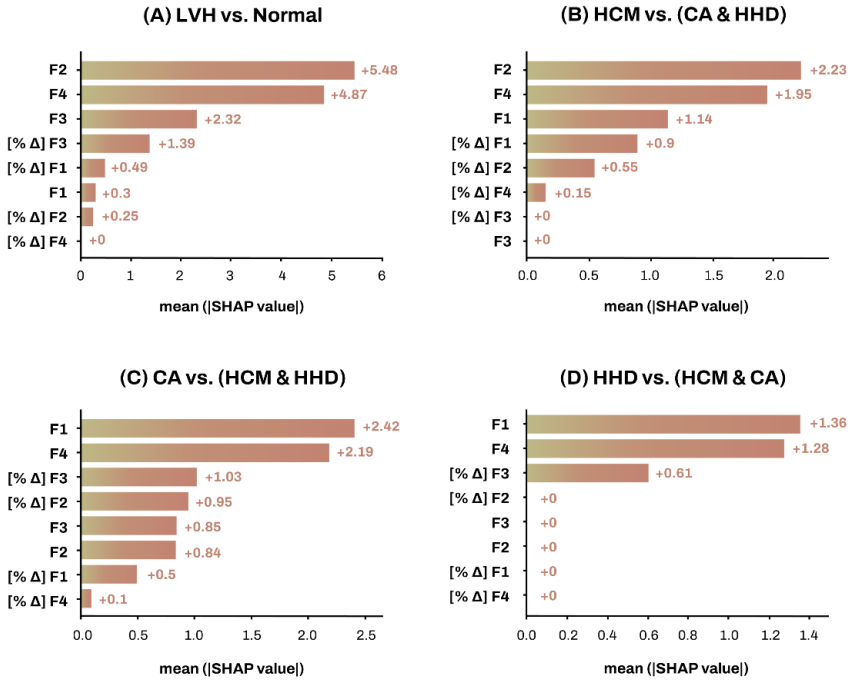

F1: Conventional Textures **F2**: Harmonization-driven Textures **F3**: Myocardial Shape **F4**: Myocardial Thickness

Abbreviations: CA, cardiac amyloidosis; HCM, hypertrophic cardiomyopathy; HHD, hypertensive heart disease; LVH, left ventricular hypertrophy; SHAP, Shapley Additive exPlanations.

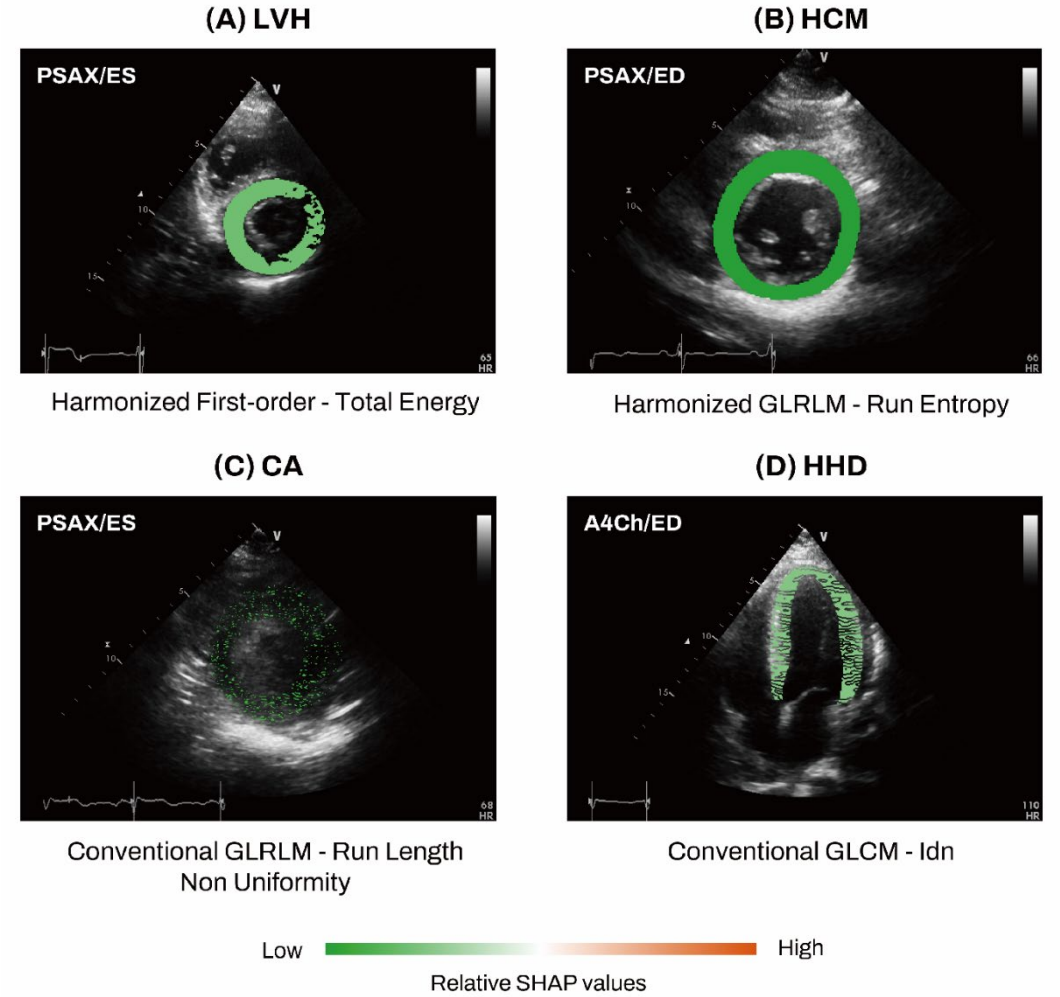

Abbreviations: A4Ch, apical four-chamber view; CA, cardiac amyloidosis; GLCM, gray level co-occurrence matrix; GLRLM, run entropy derived from a gray-level run-length matrix; ED, end-diastole; ES, end-systole; HCM, hypertrophic cardiomyopathy; HHD, hypertensive heart disease; LVH, left ventricular hypertrophy; SHAP, Shapley Additive exPlanations; PSAX, parasternal short axis view

4. DISCUSSION

This study explored the effectiveness of utilizing echocardiography-based radiomics features analyzed through ML models to enhance LVH diagnosis and differentiate its etiologies. Our approach, which integrates advanced myocardial texture analysis and geographic attributes, was thoroughly validated internally and externally, showcasing robust performance. Furthermore, enhanced by SHAP analyses, our approach also offered clinical interpretability. These findings underscore the potential clinical relevance and adaptability of our methods for practical clinical application in real-world settings.

Echocardiography is the most widely used noninvasive tool among cardiovascular imaging modalities, utilizing not only the measurements of various structural and functional parameters but also the visual assessment of morphology. Given the wide range of cardiovascular diseases which often overlap morphologies across the various etiologies, the echocardiographic assessment inevitably conveys obscure conclusions with subjective interpretations. LVH, a common cardiovascular condition, has various etiologies. HHD results from increased afterload,[32] HCM has genetic roots and may requir specific management for the complications (i.e., sudden cardiac death, heart failure, arrhythmia, etc),[33,34] and CA is the result from progressive deposition of amyloid in the extracellular matrix due to hematologic malignancy (light-chain CA) typically shows grave prognosis or other genetic and idiopathic causes (transthyretin CA) requiring specific therapy.[35,36] Despite different etiologies, morphologic similarities and the lack of pathognomonic findings often challenge accurate diagnosis by visual assessments and conventional echocardiographic evaluation. Indeed, the accuracy of human experts in differentiating the etiologies of LVH ranges from 50% to 80%.[9,10] This necessitates further diagnostics such as cardiac magnetic resonance, nuclear scintigraphy, genetic testing, and myocardial biopsy to overcome the limitations of conventional echocardiography.[6]

To improve the diagnostic process and minimize unnecessary tests, researchers have employed DL in echocardiography to detect subtle differences in LVH etiologies that are not apparent through conventional methods.[9-11] Given the reliance on subjective judgment by echocardiographic specialists,[4,6] the ability of DL to process a broader spectrum of data, including subtle characteristics missed by humans, positions it as potentially superior for LVH

detection and differential diagnosis. For instance, Yu et al. developed a semi-automatic diagnostic network based on deep learning algorithms to detect LVH and differentiate between different etiologies of LVH.[10] They use the still images of PLAX and A4Ch view and manually demarked LV myocardium for the ground truth of the segmentation network. And, Duffy et al. showed the reliability of quantifying LV dimension and wall thickness and predicting the cause of LVH using a deep learning algorithm trained by A4Ch view of echocardiogram videos.[11] The externally validated algorithm showed 0.89 of AUC in HCM and 0.83 in CA patients. Notably, Hwang et al. reported that DL-based differentiation of LVH etiology was superior to human expertise, achieving an overall accuracy of 92.3% compared to 80%, underscoring the potential benefits of DL in improving diagnostic accuracy.[9] They used a high-performance algorithm that was constructed using a hybrid CNN-long short-term memory model. However, previous efforts in applying DL encountered remarkable limitations, including the lack of multi-center cohorts and external validation.[9-11] Additionally, the critical need for interpretability, essential for securing clinical trust and facilitating wider adoption, remains largely unaddressed.

In this study, we aimed to enhance diagnostic accuracy and provide significant insight by employing echocardiography-based radiomics features. Besides DL algorithm, radiomic feature analysis offers an advantage in interpretability and allows for integrating various statistical models based on the extracted features. Instead of directly inputting echocardiographic images into a DL model, we applied AI technology for automated segmentation of the LV myocardium, extracting and analyzing a broad array of features. This approach allowed for an in-depth examination of myocardial texture and geographic features. Specifically, myocardial shape (F3) and thickness (F4) were identified as important factors in diagnosing and differentiating LVH. Myocardial thickness (F4) proved crucial across all the processes of etiologic diagnosis, while the percent change in myocardial shape ([%Δ] F3) played a significant role in differentiating CA (Fig. 8).

In the evaluation of LVH, assessing myocardial texture is an aspect that echocardiography has long attempted to characterize because of its potential value. Bhandari et al. and Pinamonti et al. tried to myocardial exture analysis in 3-D echocardiography in 1980s.[37,38] Similar with our study, there were recent studies that used echocardiography-based radiomic feature analysis to classify the various LVH etiologies.[39,40] Particularly, texture analysis has shown promise in detecting LV remodeling and differentiating transthyretic CA from other cardiomyopathy.[41,42] Despite the

historical challenges in quantifying myocardial texture changes, which often reduce diagnostic reproducibility, we address this issue by employing an AI-driven approach to automatically segment the LV myocardium, extract, and analyze texture features. Importantly, our method incorporated both conventional (F1) and novel harmonization-driven (F2) texture features, the latter designed to reduce variability across different imaging settings and vendors.[23] In our classification model, both texture features were pivotal: the harmonization-driven texture features (F2) were crucial for detecting LVH and differentiating HCM, while conventional texture features (F1) significantly helped in differentiating CA. Although geographic features played an essential role in identifying HHD, conventional texture features (F1) also extensively aided in its differentiation (Fig. 8).

This approach effectively quantifies and evaluates the impact of specific myocardial features on the detection and differentiation of LVH. By identifying which echocardiography-based radiomics features are pivotal in differentiating various cardiac conditions, our classification model gains credibility and provides deeper insights into the diagnostic process. Furthermore, the model's scalability allows it to classify unknown conditions beyond the current diagnostic scope by placing atypical cases into the "Others" category. This method enhances diagnostic safety by preventing disease misclassification. Intriguingly, as SHAP values have highlighted, divergent texture features in misclassified cases suggest the possibility of uncovering unrecognized pathophysiologies.

4.1. Limitations

This study has some limitations. First, although the training data set was multi-center-driven and the model was externally validated, it was predominantly based on data sourced from Korean patient cohorts. This could introduce ethnic biases and suggest a need for further validation across diverse demographic populations. Extending the model to include a broader range of conditions and testing it in various settings with different equipment standards will be essential to enhance its applicability and reliability. Second, our study focused on patients with advanced LVH due to HCM, CA, and HHD, which may introduce bias. Since these are cases of pathologic LVH, not only does the myocardial thickness increase, but myocardial remodeling and fibrosis also occur. Therefore, myocardial texture features could play a more significant role in

distinguishing LVH in the model. Previous studies have shown that radiomic features outperform the LV mass index in predicting LV remodeling, which supports this notion.[41] As a result, the model we developed may have limitations when applied to subclinical LVH or physiologic LVH cases (such as athlete's heart). Further studies will be necessary to validate and improve the model's capabilities for these groups. Third, our cohort did not include the rare causes of LVH, such as Fabry disease, Danon syndrome, PRKAG2 syndrome, and sarcoidosis due to their low prevalence, which complicates achieving adequate training levels. Although we incorporated an "Others" category for features not typical of the trained disease groups, further validation is required to determine how the model performs when presented with untrained disease categories. Lastly, while we have demonstrated the robustness of our model by applying it to an independent external validation set with different compositions, we acknowledge the significant challenges of lacking prospective testing and evaluation of model efficacy during actual clinical practice.[43] Plans are underway to conduct prospective studies to address this gap.

5. CONCLUSIONS

In this study, we developed an AI-based classification model that utilizes echocardiography-based radiomics to enhance the diagnosis and differentiation of LVH. The model, which was developed using data from multi-institutional cohorts and validated externally, demonstrates promising results in applying radiomic analysis to real-world clinical settings. However, its application has been primarily within a specific demographic, highlighting the need for broader testing across diverse populations to ensure its efficacy and generalizability in varied clinical settings.

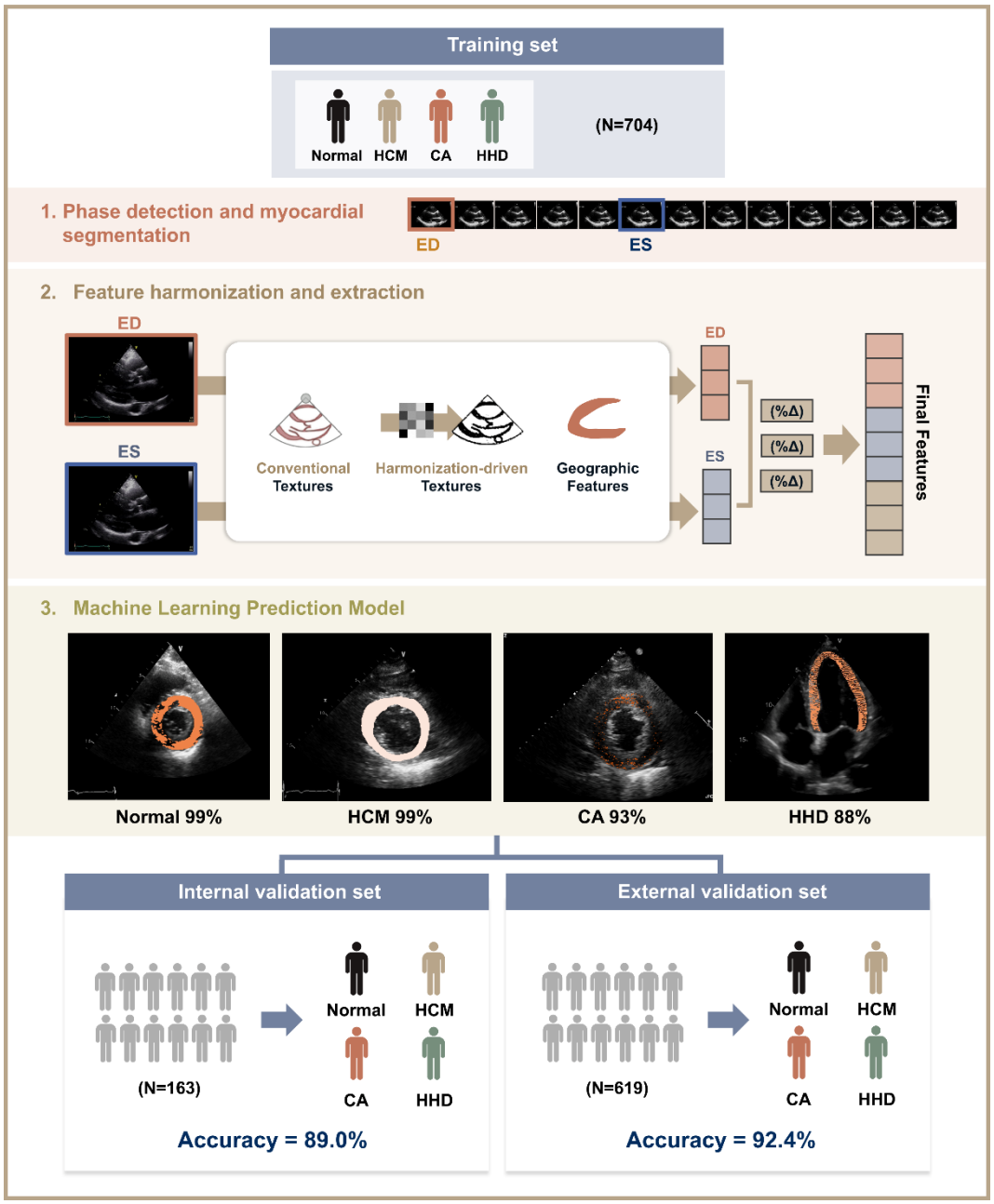

were extracted and used to develop classification models for detecting LVH and differentiating its etiologies. The performance of these models was subsequently evaluated through internal and external validation datasets.

Abbreviations: CA, cardiac amyloidosis; ED, end-diastole; ES, end-systole; HCM, hypertrophic cardiomyopathy; HHD, hypertensive heart disease; LV, left ventricular; LVH, left ventricular hypertrophy.

References

1. Cuspidi C, Facchetti R, Bombelli M, Sala C, Tadic M, Grassi G, et al. Risk of mortality in relation to an updated classification of left ventricular geometric abnormalities in a general population: the Pamela study. J Hypertens. 2015;33:2133-40.

2. Drazner MH. The progression of hypertensive heart disease. Circulation. 2011;123:327-34.

3. Ruilope LM, Schmieder RE. Left ventricular hypertrophy and clinical outcomes in hypertensive patients. Am J Hypertens. 2008;21:500-8.

4. Weidemann F, Niemann M, Ertl G, Stork S. The different faces of echocardiographic left ventricular hypertrophy: clues to the etiology. J Am Soc Echocardiogr. 2010;23:793-801.

5. Angeli F, Reboldi G, Verdecchia P. Echocardiographic left ventricular hypertrophy: implications for clinicians. J Hypertens. 2012;30:2279-84.

6. Yilmaz A, Sechtem U. Diagnostic approach and differential diagnosis in patients with hypertrophied left ventricles. Heart. 2014;100:662-71.

7. Davis A, Billick K, Horton K, Jankowski M, Knoll P, Marshall JE, et al. Artificial Intelligence and Echocardiography: A Primer for Cardiac Sonographers. J Am Soc Echocardiogr 2020;33:1061-66.

8. Kusunose K, Haga A, Abe T, Sata M. Utilization of Artificial Intelligence in Echocardiography. Circ J 2019;83:1623-29.
9. Hwang IC, Choi D, Choi YJ, Ju L, Kim M, Hong JE, et al. Differential diagnosis of common etiologies of left ventricular hypertrophy using a hybrid CNN-LSTM model. Sci Rep. 2022;12:20998.

9. Yu X, Yao X, Wu B, Zhou H, Xia S, Su W, et al. Using deep learning method to identify left ventricular hypertrophy on echocardiography. Int J Cardiovasc Imaging. 2022;38:759-69.

10. Duffy G, Cheng PP, Yuan N, He B, Kwan AC, Shun-Shin MJ, et al. High-Throughput Precision Phenotyping of Left Ventricular Hypertrophy With Cardiovascular Deep Learning. JAMA Cardiol. 2022;7:386-95.

11. Park JE, Park SY, Kim HJ, Kim HS. Reproducibility and Generalizability in Radiomics Modeling: Possible Strategies in Radiologic and Statistical Perspectives. Korean J Radiol 2019;20:1124-37

12. Open AI Dataset Project (AI-Hub). National Information Society. https://aihub.or.kr/.

13. Korea National Standard Cardiovascular Database and Reference. Korea Research Institute of Standards and Science. https://www.srd.re.kr/css/ index.do

14. Sengupta PP, Shrestha S, Berthon B, Messas E, Donal E, Tison GH, et al. Proposed Requirements for Cardiovascular Imaging-Related Machine Learning Evaluation (PRIME): A Checklist: Reviewed by the American College of Cardiology Healthcare Innovation Council. JACC Cardiovasc Imaging. 2020;13:2017-35.

15. Jeon J HS, Yoon YE, Kim J, Jeong H, Jeong D, Jang Y, et al. Improving Out-of-Distribution Detection in Echocardiographic View Classication through Enhancing Semantic Features. arXiv preprint arXiv:230816483 2023. doi: 10.48550/arXiv.2308.16483

16. Jang Y, Choi H, Yoon YE, Jeon J, Kim H, Kim J, et al. An Artificial Intelligence-Based Automated Echocardiographic Analysis: Enhancing Efficiency and Prognostic Evaluation in Patients With Revascularized STEMI. Korean Circ J. 2024;54:e103. doi: 10.4070/kcj.2024.0060

17. Park J, Jeon J, Yoon YE, Jang Y, Kim J, Jeong D, et al. Artificial intelligence-enhanced automation of left ventricular diastolic assessment: a pilot study for feasibility, diagnostic validation, and outcome prediction. Cardiovasc Diagn Ther. 2024;14:352-66.

18. Jaderberg M, Simonyan K, Zisserman A, Kavukcuoglu K. Spatial Transformer Networks. Adv Neur In. 2015;28.

19. Ostvik A, Salte IM, Smistad E, Nguyen TM, Melichova D, Brunvand H, et al. Myocardial Function Imaging in Echocardiography Using Deep Learning. Ieee T Med Imaging. 2021;40:1340-51.

20. van Griethuysen JJM, Fedorov A, Parmar C, Hosny A, Aucoin N, Narayan V, et al. Computational Radiomics System to Decode the Radiographic Phenotype. Cancer Res. 2017;77:e104-7.

21. Woo S, Debnath S, Hu R, Chen X, Liu Z, Kweon IS, et al. ConvNeXt V2: Co-designing and Scaling ConvNets with Masked Autoencoders. arXiv:230100808. 2023.

22. Lee JN, Jeong DW, Jang YG, Jeong SH, Jung TG, Yoon YE, et al. Self supervised convolutional kernel based handcrafted feature harmonization: Enhanced left ventricle hypertension disease phenotyping on echocardiography. arXiv preprint arXiv:231008897. 2023.

23. Chen Q, Pan T, Wang YN, Schoepf UJ, Bidwell SL, Qiao H, et al. A Coronary CT Angiography Radiomics Model to Identify Vulnerable Plaque and Predict Cardiovascular Events. Radiology. 2023;307:e221693.

24. Kursa MB, Rudnicki WR. Feature Selection with the Boruta Package. J Stat Softw. 2010;36:1-13.

25. Al'Aref SJ, Singh G, Choi JW, Xu Z, Maliakal G, van Rosendael AR, et al. A Boosted Ensemble

Algorithm for Determination of Plaque Stability in High-Risk Patients on Coronary CTA. JACC Cardiovasc Imaging. 2020;13:2162-73.

26. Ke G, Finley T, Wang T, Chen W, Ma W, Ye Q, et al. LightGBM: A Highly Efficient Gradient Boosting Decision Tree. Adv Neural Inf Process Syst. 2017;30:3149–57.

27. Chawla NV, Bowyer KW, Hall LO, Kegelmeyer WP. SMOTE: Synthetic minority over-sampling technique. J Artif Intell Res. 2002;16:321-57.

28. Youden WJ. Index for rating diagnostic tests. Cancer. 1950;3:32-35.

29. Luo X, Piao S, Li H, Li Y, Xia W, Bao Y, et al. Multi-lesion radiomics model for discrimination of relapsing-remitting multiple sclerosis and neuropsychiatric systemic lupus erythematosus. Eur Radiol. 2022;32:5700-10.

30. Scott M. Lundberg S-IL. A unified approach to interpreting model predictions. Proceedings of the 31st International Conference on Neural Information Processing Systems. 2017:4768–77.

31. Schirmer H, Lunde P, Rasmussen K. Prevalence of left ventricular hypertrophy in a general population; The Tromso Study. Eur Heart J. 1999;20:429-38.

32. Maron MS, Hellawell JL, Lucove JC, Farzaneh-Far R, Olivotto I. Occurrence of Clinically Diagnosed Hypertrophic Cardiomyopathy in the United States. Am J Cardiol. 2016;117:1651-54.

33. Moon I, Lee SY, Kim HK, Han KD, Kwak S, Kim M, et al. Trends of the prevalence and incidence of hypertrophic cardiomyopathy in Korea: A nationwide population-based cohort study. PLoS One. 2020;15:e0227012.

34. Kittleson MM, Maurer MS, Ambardekar AV, Bullock-Palmer RP, Chang PP, Eisen HJ, et al, American Heart Association Heart F, Transplantation Committee of the Council on Clinical C. Cardiac Amyloidosis: Evolving Diagnosis and Management: A Scientific Statement From the American Heart Association. Circulation. 2020;142:e7-22.

35. Arbelo E, Protonotarios A, Gimeno JR, Arbustini E, Barriales-Villa R, Basso C, et al. 2023 ESC Guidelines for the management of cardiomyopathies. Eur Heart J. 2023;44:3503-626

36. Bhandari AK, Nanda NC. Myocardial texture characterization by two-dimensional echocardiography. Am J Cardiol. 1983;51:817-25.

37. Pinamonti B, Picano E, Ferdeghini EM, Lattanzi F, Slavich G, Landini L, et al. Quantitative texture analysis in two-dimensional echocardiography: application to the diagnosis of myocardial amyloidosis. J Am Coll Cardiol. 1989;14:666-71.

38. Yu F, Huang H, Yu Q, Ma Y, Zhang Q, Zhang B. Artificial intelligence-based myocardial texture analysis in etiological differentiation of left ventricular hypertrophy. Ann Transl Med.

2021;9:108.

39. Zhang X, Liang T, Su C, Qin S, Li J, Zeng D, Cai Y, Huang T, Wu J. Deep learn-based computer-assisted transthoracic echocardiography: approach to the diagnosis of cardiac amyloidosis. Int J Cardiovasc Imaging. 2023;39:955-65.

40. Hathaway QA, Yanamala N, Siva NK, Adjeroh DA, Hollander JM, Sengupta PP. Ultrasonic Texture Features for Assessing Cardiac Remodeling and Dysfunction. J Am Coll Cardiol. 2022;80:2187-201.

41. Datar Y, Cuddy SAM, Ovsak G, Giblin GT, Maurer MS, Ruberg FL, et al. Myocardial Texture Analysis of Echocardiograms in Cardiac Transthyretin Amyloidosis. J Am Soc Echocardiogr. 2024;37:570-73.

42. Wu E, Wu K, Daneshjou R, Ouyang D, Ho DE, Zou J. How medical AI devices are evaluated: limitations and recommendations from an analysis of FDA approvals. Nat Med. 2021;27:582-84.

인공지능을 활용한 심초음파 기반 방사선 영상 (Radiomics) 특징 분석을 통한 심근 비대 감지 및 병인 구별

심초음파검사는 좌심실비대(LVH) 검출에 핵심적이지만, 원인 감별에는 어려움이 있다. LVH 평가를 향상시키기 위해, 우리는 심초음파 기반 방사선체학을 이용한 인공지능(AI) 알고리즘 개발을 목표로 했다. 이 알고리즘은 심초음파 영상을 바탕으로 LVH 를 검출하고 비대성심근병증(HCM), 심장 아밀로이드증(CA), 고혈압성심질환(HHD) 등 주요 원인들을 감별하도록 설계되었다.

개발 데이터셋은 다양한 의료센터에서 수집되었고(867명), 독립적인 외부 검증셋은 단일 3차 의료센터에서 확보되었다(619명). 4가지 기본 심초음파 영상에 대한 방사선체학적 특징 분석을 통해 기존 방식과 조화화 기반 심근 질감을 추출했다. 심근 모양과 두께 같은 심근 지리학적 특징도 주요 변수로 활용되었다. 분류 알고리즘을 개발하고, 각 변수의 기여도는 새플리 가법 설명으로 평가했다.

내부 검증에서 분류 모델은 곡선하면적(AUC) 1.00 (95% 신뢰구간 [CI], 1.00–1.00)으로 LVH를 신뢰성 있게 검출했다. 원인 감별에서도 강력한 성능을 보여, HCM은 AUC 0.97 (95% CI, 0.94–0.99), CA는 0.95 (95% CI, 0.90–0.99), HHD는 0.86 (95% CI, 0.78–0.93)을 달성했다. 외부 검증에서도 이러한 결과가 일관되게 나타나, HCM은 AUC 0.96 (95% CI, 0.92–0.98), CA는 0.89 (95% CI, 0.83–0.93), HHD는 0.86 (95% CI, 0.81–0.91)을 기록했다. 특히 조화화 기반 질감은 HCM 감별에서 핵심적 역할을 했으며, 기존 질감과 심근 두께는 CA와 HHD 감별에 영향을 미쳤다.

이 연구는 AI가 강화된 심초음파 기반 방사선체학이 LVH와 그 원인들을 효과적으로 식별함을 확인하며, LVH 평가에서 AI 기반 질감 및 지리학적 분석의 잠재력을 부각시킨다.

핵심되는 말 : 심초음파 기반 방사선체학, 인공지능, 심근비대